CHALMERS

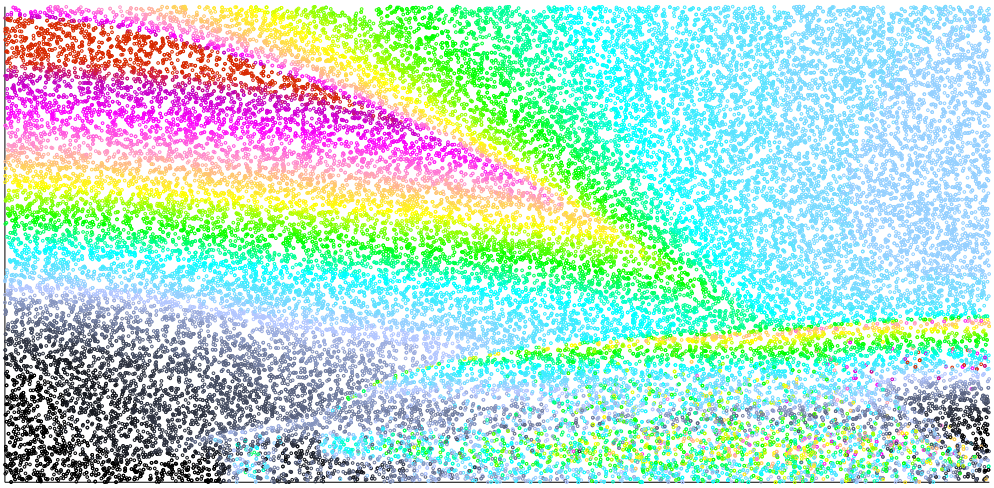

Magnetic and Chemical Contributions to Interface Free Energy

A Monte Carlo Simulation Study

Bachelor's thesis in Computational Physics

MATTIAS ÅNGQVIST
ERIK FRANSSON
ERIK JEDVIK
JOHAN LÖVGREN

Department of Applied Physics
Division of Materials and Surface Theory
CHALMERS UNIVERSITY OF TECHNOLOGY
Gothenburg, Sweden 2012

Bachelor's thesis TIFX02-12-13

BACHELOR'S THESIS IN COMPUTATIONAL PHYSICS

Magnetic and Chemical Contributions to Interface Free Energy

A Monte Carlo Simulation Study

MATTIAS ÅNGQVIST
ERIK FRANSSON
ERIK JEDVIK
JOHAN LÖVGREN

Department of Applied Physics
Division of Materials and Surface Theory
CHALMERS UNIVERSITY OF TECHNOLOGY

Gothenburg, Sweden 2012

Magnetic and Chemical Contributions to Interface Free Energy
A Monte Carlo Simulation Study
MATTIAS ÅNGQVIST
ERIK FRANSSON
ERIK JEDVIK
JOHAN LÖVGREN

Bachelor's thesis TIFX02-12-13
ISSN 1654-4676
Department of Applied Physics
Division of Materials and Surface Theory
Chalmers University of Technology
SE-412 96 Gothenburg
Sweden
Telephone: +46 (0)31-772 1000

Cover:
The standard deviation of the total energy of an iron-chromium alloy obtained through Monte Carlo simulations plotted as a function of atomic fraction chromium versus temperature in reduced units.

Chalmers Reproservice
Gothenburg, Sweden 2012

Magnetic and Chemical Contributions to Interface Free Energy
A Monte Carlo Simulation Study
Bachelor's thesis in Computational Physics
MATTIAS ÅNGQVIST
ERIK FRANSSON
ERIK JEDVIK
JOHAN LÖVGREN
Department of Applied Physics
Division of Materials and Surface Theory
Chalmers University of Technology

Abstract

This report studies implications of chemical and magnetical contributions to a Fe-Cr alloy using Monte Carlo simulations of a modified Ising Model. Through order parameter the properties of the alloy has been characterised and the phase diagram of Fe-Cr , which exhibits the main characteristics of the experimentally obtained phase diagram has been constructed.

For low temperatures and intermediate concentrations a new ordered phase, which resembles the ternary Heusler alloy, has been found together with the corresponding phase boundary.

The Variance Constrained Semi-Grand Canonical ensemble was successfully applied to compute the interface free energy as a function of concentration and the value of the interface free energy in the [100]-direction has been computed.

From the interface free energy the miscibility gap, where phase separation between chromium-rich and iron-rich clusters form, has been constructed. Also the spinodal, the limit of where metastable phases can exist, has been found. A pronounced size dependence of the difference between spinodals and binodals has been found and the assumption that the difference at system size of 20^3 is negligible is proven to be wrong.

Keywords: Ising model, Monte Carlo simulations, Thermodynamics, Interface Free Energy, Fe-Cr

Preface

This is the final report of the bachelors project "Hands-on statistical mechanics: A primer in free energy calculation" supervised by Paul Erhart at the institution of Applied Physics at Chalmers University of Technology.

Two significant parts of the project, which are not mentioned further in the report, have consisted of literature studies and the writing of a working program code in the C++.

The report is written under the assumption that the reader is familiar with basic thermodynamics, statistical physics and solid state physics, but a short summary can be found in the appendix. Chapters 2 and 3 are intended for a junior reader and explains the theory behind interface free energy and Monte Carlo simulations respectively. The project has been split in two parts, chapter 4 deals with order parameters and chapter 5 the interface free energy. In chapter 6 and 7 the results are discussed and summarised.

Acknowledgements

We would like to thank our supervisor Assistant Professor Paul Erhart for inspiration, guidance and patience without which this project would never have been manageable, Professor Göran Wahnström for his support and encouragement and Jan-Olof Nilsson at Sandvik AB for insight into industrial applications.

Contents

1 Introduction

Steel manufacturing has formed the backbone of Swedish industry for more than a century and stainless steels in particular have seen Sweden rise to world prominence in materials engineering and design. Traditionally steels have been developed by phenomenological means but the advent of powerful computers has made theoretical and computational means of steel development possible, often by the Calphad approach [1]. Theoretical understanding of phase equilibria and knowledge and development of computational methods in thermodynamics are thus of paramount importance for the development of new steel grades and for the continued prosperity of Sweden.

The Iron-Chromium system, which forms the basis of all stainless steels, has attracted an increasing amount of attention lately owing partly to the high cost of nickel [2] which has favoured nickel free ferritic stainless steels, but also due to its low thermal expansion making it suitable for high temperature applications. In particular they are used in the nuclear industry due to the low swelling and high corrosion resistance under extreme conditions [3].

In addition to being a vital part of Swedish industry and interesting in engineering applications the Fe-Cr alloy also shows some features of great theoretical interest and significance. The phase diagram of Fe-Cr exhibits a miscibility gap at low temperatures where Fe-Cr decomposes into Fe-rich and Cr-rich fractions [4], a decomposition which often occurs via spinodal decomposition [5]. As a consequence high-chromium steels, with more than 12 wt% Cr, are known to suffer from 475°C embrittlement [6].

Another most interesting and unusual feature is the large asymmetry between the Fe and Cr-rich sides of the miscibility gap, with the Fe-rich side exhibiting a much larger solubility. This behaviour has been traced to a negative enthalpy of mixing for moderate concentrations of chromium in the ferromagnetic model [7, 8, 9]. However, this has been pursued further by Korzhavyi *et al.* [10] who claim that the ferromagnetic model cannot be used at temperatures above the Curie temperature, and have applied more sophisticated methods. However, below the Curie temperature, their results are still in good agreement despite the use of different methods.

Many of the interesting properties of the Fe-Cr system stem from the ferromagnetic nature of iron and the antiferromagnetic nature of chromium and do not require advanced *ab initio* calculations but can, at least qualitatively be understood from a simple Ising Model [11], but also within a moderate error margin computed with a modified Ising Model [12].

1.1 Purpose

The purpose of the present work is to study how the simple Ising model can explain many of the most important features of a ferromagnetic model and to obtain the interface free energy of a binary alloy using the Monte Carlo Metropolis algorithm [13] in a finite size system.

1.2 Limitations

This work focuses its attention to the Ising model due to its simplicity and wide applicability to a variety of phenomena. However, the Ising model is a lattice based model and does not take lattice vibrations into account, nor does it account for misfits due to different lattice parameters of the different phases nor to thermal expansion. Being a ferromagnetic model, the Ising model cannot explain paramagnetic interactions and only phenomena below the critical temperatures can be described. Further more, the Ising model is a classical, as opposed to quantum mechanical, mean field approximation and since magnetism is a purely quantum mechanical phenomenon certain correlation effects as well as local disordered moments are disregarded.

2 Theory

Every thermodynamic system strives to minimise its free energy.[1] But since there is a contribution both from the enthalpy H and the entropy S, the free energy does not assume a minimum value for the lowest possible enthalpy other than at $T = 0$. With increasing temperature the entropy contribution increases and a solid substance at a high enough temperature even dissolves into liquid phase in order to increase its entropy.

2.1 Free Energy of a Binary Mixture

For a real solid solution the enthalpy H is usually positive and the typical behaviour of H and $-TS$ as functions of concentration for a symmetric solution are seen in Figure 2.1. For high temperature the case is simple. The solution assumes the homogeneous configuration that minimises the free energy at the given concentration. For lower temperature the situation is more subtle. The free energy of a homogeneous solution (dashed circle in Figure 2.2) is not the lowest possible free energy of the system. A lower free energy may be attained by formation of two different phases (filled circles), one α-phase rich in A with a solution of B and one β-phase rich in B with a solution of A (Figure 2.2). The free energy thus attained will be ΔG_v less than the random solution.

2.2 Interface Free Energy

However, not all the energy in the random solution ΔG_v is available to the system since phase separation involves interface formation which is associated with an energy cost. For a system containing an interface of area A and interface free energy per unit area γ the total free energy is given by

$$G = G_0 + A\gamma \tag{2.1}$$

where G_0 is the free energy of the system assuming all the material in the system has bulk properties. $\Delta G = A\gamma$ is thus the *excess* free energy due to the fact that some material lies in or close to an interface. It is also the work that has to be done to create such an interface. One can show that the free energy $\gamma\,[\mathrm{Jm}^{-2}]$ exerts a surface tension of $\gamma\,[\mathrm{Nm}^{-1}]$.

In a solid the free energy associated with the formation of an interface from a random solution will have three different contributions: (i) the creation of a precipitate of volume V will cause a reduction of the free energy by $V\Delta g_v$, (ii) the creation of an interface will increase the free energy by $A\gamma$ and (iii) if the precipitate does not have the same structure or lattice parameter

[1] We will generally not make a distinction between the Helmholtz free energy $F = E - TS$ and the Gibbs free energy $G = E + PV - TS$ since we assume that the change in volume is negligible and simply refer to the free energy $F = G$. In this section however, we will write G since the Gibbs free energy is more general in this context.

and does not fit perfectly into the space there will be an increase of the free energy by $V\Delta g_s$. This gives a total free energy change of

$$\Delta G = -V\Delta g_v + A\gamma + V\Delta g_s \tag{2.2}$$

The *interface free energy* γ is of great importance for the understanding of nucleation and precipitation growth in solids. In general the interface free energy γ is not isotropic but will be different in different direction, e.g. $\gamma_{[100]} \neq \gamma_{[110]} \neq \gamma_{[111]}$.

Ignoring this variation of γ with orientation and assuming a spherical precipitate with radius r equation (2.2) can be written

$$\Delta G = -\frac{4\pi r^3}{3}(\Delta g_v - \Delta g_s) + 4\pi r^2\gamma \tag{2.3}$$

This is plotted in Figure 2.3. Note that the effect of misfit strain g_s is to reduce the effective driving force for the transformation. Straight-forward differentiation of (2.3) yields the critical radius of nucleation

$$r^* = \frac{2\gamma}{\Delta g_v - \Delta g_s} \tag{2.4}$$

and the threshold energy of nucleation

$$\Delta G^* = \frac{16\pi\gamma^3}{3(\Delta g_v - \Delta g_s)} \tag{2.5}$$

The process of nucleation and growth prevails inside the miscibility gap in the region where the second derivative of the free energy is positive. A small perturbation in local concentration increases the total free energy and the formation of a precipitate is only possible if the thermal energy of the system is high enough to overcome the activation energy barrier. This process of uphill diffusion is shown in Figure 2.4.

Beyond the point where the second derivative of the free energy changes sign even the slightest perturbation in local concentration will lower the free energy and precipitation occurs without barrier of nucleation. This process is called *spinodal decomposition* and the concentrations where $\frac{\partial^2 G}{\partial c^2} = 0$ are called *spinodals*.

The criterion usually applied for obtaining the miscibility gap is that $\partial\Delta G/\partial c = 0$ on the boundary. The concentrations where the first derivative of the free energy is zero are called the *binodals*. The region between the binodals and the spinodals is a metastable phase and nuclei will constantly form and dissolve.

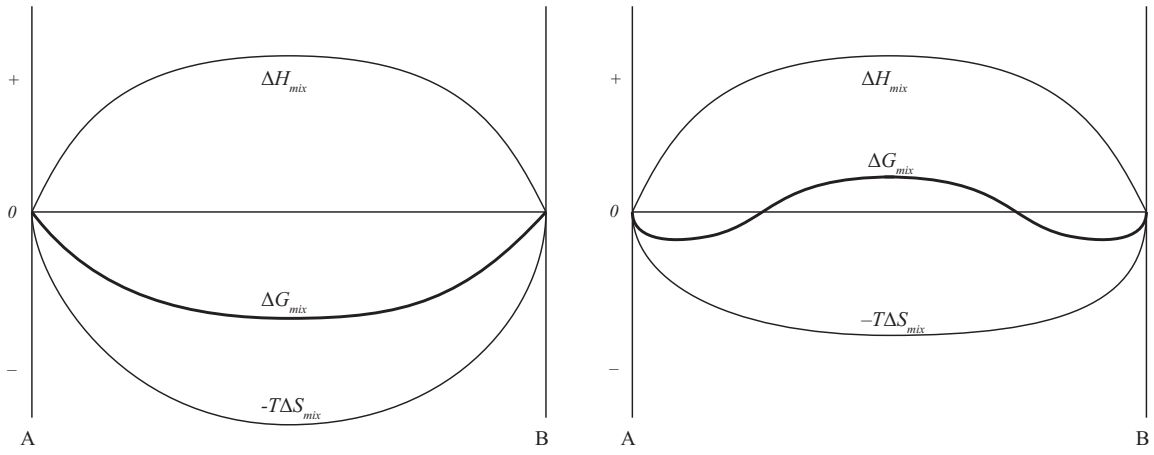

Figure 2.1: *The free energy at high temperature (a) and low temperature (b)*

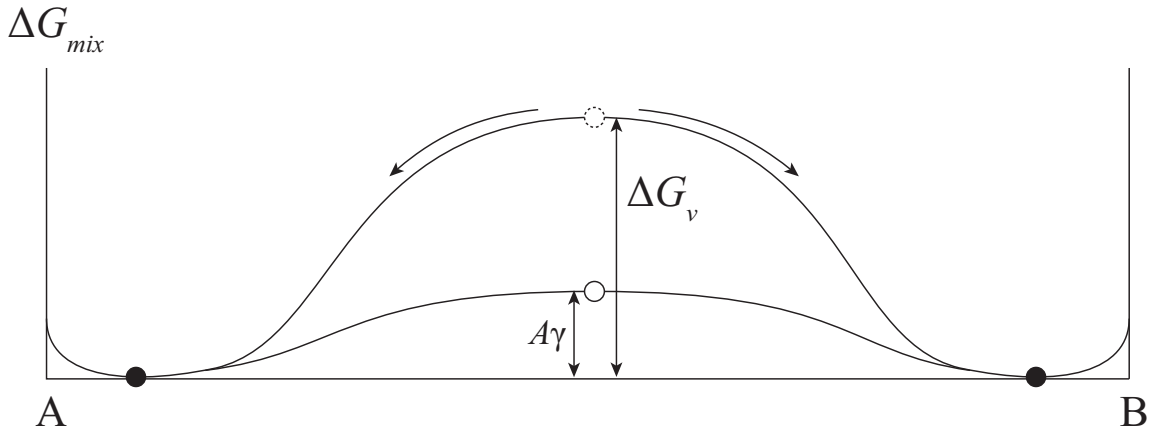

Figure 2.2: *A homogeneous solution (dashed circle) can lower its free energy by ΔG_{RS} by separation of phases (filled circles). However, if the formation of interfaces is taken into account there is a cost of $\Delta G_\gamma = A\gamma$ in formation of a precipitate and the free energy can only be lowered by $\Delta G_{RS} - A\gamma$.*

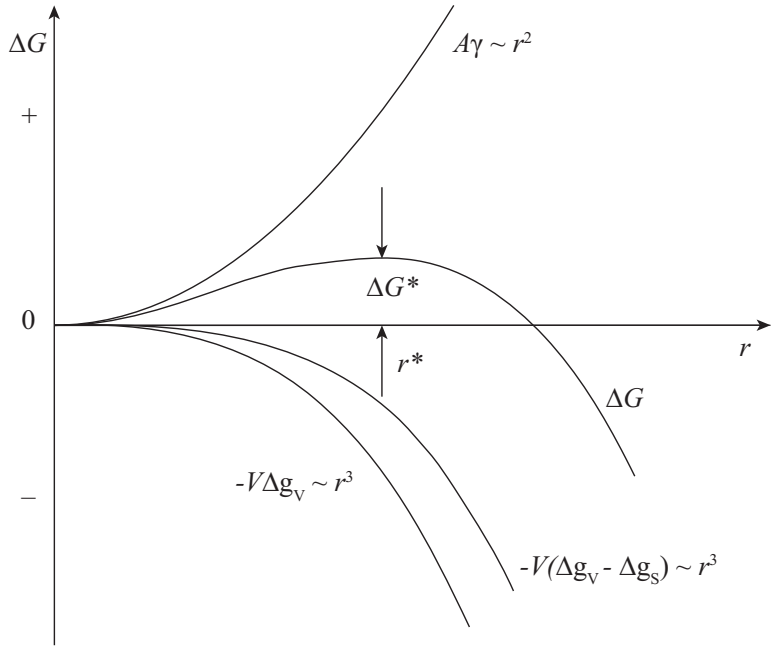

Figure 2.3: *The variation of ΔG as a function of radius r. The critical radius r^* and activation energy ΔG^* are marked in the figure. Redrawn after [14].*

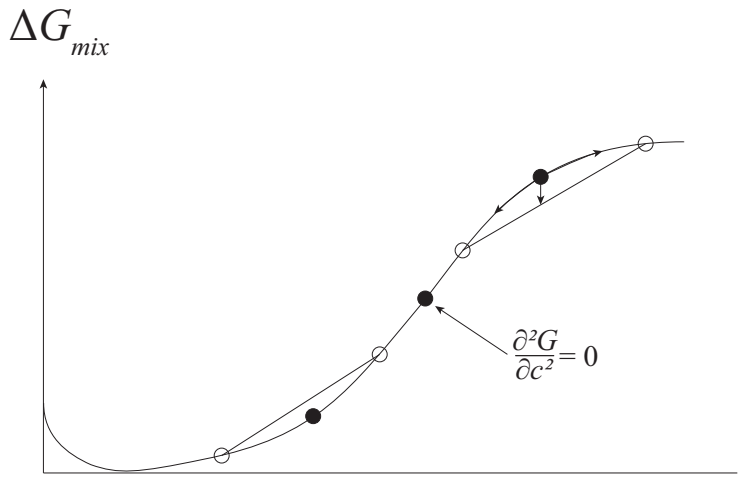

Figure 2.4: *Uphill diffusion requires an activation energy in the region to the left where $\frac{\partial^2 G}{\partial c^2} > 0$ but between the spinodals, where $\frac{\partial^2 G}{\partial c^2} > 0$ even the slightest perturbation will generate a decrease of the total free energy and there is no barrier against precipitation.*

3 Method

3.1 The Ising Model

The Ising model is one of the simplest models used in the study of magnetisation in materials [15, 16]. The atoms are assumed frozen in a lattice and assigned a magnetic spin σ restricted to be either up $(+1)$ or down (-1). Although the Ising model in itself does not prohibit long range interaction, we will only be considering nearest and second nearest neighbours interaction. If $\sigma_i = \pm 1$ represents the spin of the atom, the original Ising model simply states that, for an interaction energy ε the energy of certain site i is given by

$$\mathcal{H}_i = -\varepsilon \sum_j \sigma_i \sigma_j \tag{3.1}$$

where the sum over j is carried out over the neighbours. The total energy of the system is then given as one half of the sum over all lattice sites i. The coefficient ε is determined by the choice of units and can be calibrated from experimental data. In general the temperature T will be measured in units of ε/k_B. We will for simplicity choose $\varepsilon = 1$ and $k_B = 1$.

3.1.1 Modified Ising model

The original Ising model only allows for one type of atom and in order to take the interaction between iron and chromium into account we will use the modified and extended Ising model proposed by Ackland [11]. In order to take the ferromagnetic nature of iron $(\varepsilon > 0)$ and the antiferromagnetic nature of chromium $(\varepsilon < 0)$ into account we assign to every lattice point an atom and a spin labelled S_i and σ_i respectively, where S_i represents the type of atom, -1 for iron and $+1$ for chromium, and $\sigma_i = \pm 1$ represents the spin of the atom.

The Hamiltonian (3.2) of this model is given by a ferromagnetic or antiferromagnetic first part and a second part of Fe-Cr interaction where the sum goes over all neighbours j. As before the total energy of the system is given by one half of the sum over all lattice sites i.

$$\mathcal{H}_i = \sum_j [(S_i + S_j)\sigma_i\sigma_j/2 + (1 - S_iS_j)\sigma_i\sigma_j/2] \tag{3.2}$$

3.2 The Monte Carlo Method

To compute the partition function $Z = \sum e^{-\beta U}$, which is the sum over all possible configurations, is a formidable task. Only the one-dimensional case, solved by Ernst Ising and the two-dimensional case, solved by Lars Onsager, are analytically solvable [17]. However, there are numerical methods available. One numerical method which has proven efficient is the Monte Carlo method introduced by John von Neumann and refined by Metropolis *et al.* [13].

3.2.1 The original Monte Carlo Method

In the original Monte Carlo method the partition function is approximated by randomly sampling as many states as possible and computing the Boltzmann factor for these states. However, this brute force method is bound to fail since only a tiny number of possible states can be computed.

3.2.2 Importance Sampling

The Metropolis method is a numerically cheaper and faster way to find the most likely configurations. The idea is to sample only states which have a reasonable probability of occurring. To illustrate this let us study the one dimensional integral $I = \int_0^1 f(x)\,\mathrm{d}x = \langle f(x) \rangle$ which can be evaluated as the average value of the function computed at points uniformly distributed along the interval times the length of the interval. Now, if f is a rapidly varying function it can be advantageous to rewrite I through the identity

$$I = \int_0^1 f(x)\,\mathrm{d}x = \int_0^1 \frac{f(x)}{w(x)} w(x)\,\mathrm{d}x = \int_0^1 \frac{f(x)}{w(x)}\,\mathrm{d}u \tag{3.3}$$

where $w = \mathrm{d}u/\,\mathrm{d}x$ is a non-negative function implying that u is monotonically increasing. If w is chosen so that $f(x) \approx w(x)$ the integral can be evaluated through N random values of u randomly distributed in the interval $[0, 1]$.

$$I = \int_0^1 f(x)\,\mathrm{d}x = \left\langle \frac{f(x)}{w(x)} \right\rangle \approx \frac{1}{N} \sum_{i=1}^{N} \frac{f(x)}{w(x)} \tag{3.4}$$

To stress the advantage of this method let us construct the variance σ_I^2 defined as

$$\sigma_I^2 = \frac{1}{N} \left[\left\langle \left(\frac{f}{w} \right)^2 \right\rangle - \left\langle \frac{f}{w} \right\rangle^2 \right] \tag{3.5}$$

Equation (3.5) shows that (i) the variance goes as $1/N$, implying that better accuracy can be achieved through a greater number of samplings and (ii) that if we could choose $w = f$ the variance would vanish altogether.

Unfortunately there is no equivalent to the transformation (3.3) in higher dimension configuration space, in fact we don't even know the function we want to sample since we don't know the multiplicity of each configuration. Otherwise there would hardly be any need for computer simulations.

3.2.3 The Metropolis algorithm

The Metropolis algorithm does not provide a solution to this problem but handles the fact that the integral of interest is the mean value of the type

$$\langle E \rangle = \frac{\int E(\mathbf{x}^d) e^{\left[-\beta U(\mathbf{x}^d)\right]} \, \mathrm{d}\mathbf{x}}{\int e^{\left[-\beta U(\mathbf{x}^d)\right]} \, \mathrm{d}\mathbf{x}} \tag{3.6}$$

i.e. the ratio of two integrals. Let us as customary denote the denominator as Z. Then the ratio $e^{(-\beta U)}/Z$ is just the probability density of finding the system in configuration $\mathbf{x}^d$. If we thus can generate random numbers n_i that follow this distribution we can approximate the integral as

$$\langle E \rangle \approx \frac{1}{N} \sum_{i=1}^{N} n_i E(\mathbf{x}_i^d) \tag{3.7}$$

The problem is that Z is still unknown, because the number of configurations, $\mathbf{x}^d$, which correspond to the same energy is unknown. However, since Z is a common term the relative probabilities of visiting different points in configuration space can be computed. This way the factors Z cancel each other and the relative probability being the Boltzmann factor $e^{-\beta \Delta U}$. This is the basic idea of the Metropolis scheme.

First a random initial configuration $\mathbf{x}_o^N$ with subindex o for old has to be generated. Then a new configuration $\mathbf{x}_n^N$ is generated by adding a small random displacement. This is called a *trial move*. The corresponding Boltzmann factors are $e^{-\beta U(\mathbf{x}_o^N)}$ and $e^{-\beta U(\mathbf{x}_n^N)}$. To determine whether or not to keep the new configuration the average probability of finding a configuration n should be proportional to the probability distribution n_i.

If a very large number of simulations is carried out, very large being a number well above the number of accessible states, the number of simulations m that sample a configuration i should be proportional to the thermodynamic probability n of finding the state in that configuration, that is $m_i \propto n_i = e^{-\beta U_i}/Z$. In addition, when such a state is reached, that state should not be destroyed. In practise this means that in equilibrium the average number of accepted moves from one state i to another f should exactly equal the number of moves from state f to state i. This condition

$$n_i \mathcal{P}_{i \to f} = n_f \mathcal{P}_{f \to i} \tag{3.8}$$

is called detailed balance. Let us denote the probability of accepting a single trial move $\mathcal{A}_{i \to f}$ then the acceptance probability of one trial move has to be proportional to the probability of moving in a sequence, called a *Markov chain* between these states $\mathcal{P}_{i \to f} \propto \mathcal{A}_{i \to f}$ such that

$$n_i \mathcal{A}_{i \to f} = n_f \mathcal{A}_{f \to i} \tag{3.9}$$

$$\frac{\mathcal{A}_{i\to f}}{\mathcal{A}_{f\to i}} = \frac{n_f}{n_i} = e^{-\left(\beta U_i - \beta U_f\right)} = e^{-\beta\Delta U} \tag{3.10}$$

Clearly the probability cannot exceed unity so if $\Delta U > 0$ the probability has to be set to 1. The acceptance probability of a new state is thus computed as $\min\{1, e^{-\beta\Delta U}\}$, where ΔU is the difference in energy between the old and the new configuration.

If the system consists of N particles a trial move consists of either a random displacement or a compositional change of one particle. N such trial moves comprise a *Monte Carlo step*. After each MC step the value A_i of some parameter, e.g. the total energy, the concentration or, as in the case with the magnetic model, the magnetisation order parameter is recorded. The macroscopic thermodynamic quantity is computed as the mean value

$$\langle A \rangle = \frac{1}{M_C} \sum_{i=1}^{M_C} A_i \tag{3.11}$$

where M_C is the number of MC steps.

3.3 Monte Carlo sampling in Thermodynamic Ensembles

Assuming a system in thermal equilibrium, the physical quantities describing the system macroscopically or controlling the system externally are called *system parameters*. Every set of system parameters correspond to a set of allowed microscopic states. Different experimental circumstances correspond to different system parameters being fixed. These correspond to different *ensembles*.[1] The fundamental postulate of statistical physics is that all microscopic states corresponding to a certain value of the system parameters are equally probable and that every configuration is equally likely to be visited in the course of time (the ergodic hypothesis), which leads to the conclusion that the time average $\bar{A} = \lim_{T\to\infty} \frac{1}{T} \int_0^T A(t)\,\mathrm{d}t$ is identical to the expectation value $\langle A \rangle = \sum_i A_i \mathcal{P}(A_i)$. In order to determine the probability distribution $\mathcal{P}(A_i)$, we now consider a system of N particles with volume V, where each particle has a spin of value 0 or 1. Denote a configuration of this system $(\mathbf{x}^{3N}, \sigma^N)$, where $\mathbf{x}^{3N}$ is the $3N$-dimensional vector describing the position of each particle and σ^N is the corresponding N-dimensional spin. The number of particles with spin 1 is then $n = \sum_{i=1}^{N} \sigma_i$ and their concentration is $c = n/N$. The energy of the system can be written $U(\mathbf{x}^{3N}, \sigma^N)$.

3.3.1 Canonical Ensemble

For a system of two types of particles the partition function for the canonical ensemble at temperature T with continuous degrees of freedom is defined as

$$Z_C(c, \mathcal{N}) = \lambda_1^{-3(N-n)} \lambda_2^{-3n} \frac{1}{n!(N-n)!} \int e^{-\beta U(\mathbf{x}^{3N}, \sigma^N)}\,\mathrm{d}^{3N}\mathbf{x} \tag{3.12}$$

[1] The system parameters defining different ensembles are discussed in appendix A.

where $\beta = 1/k_B T$, $\lambda_i = \sqrt{2\pi\hbar^2/m_i k_B T}$ and $\mathcal{N} = \{N, V, T\}$ is the set of independent thermodynamic variables. The probability distribution n_i for a Monte Carlo simulation in this ensemble is then

$$\mathcal{P}_C(\mathbf{x}^{3N}, \sigma^N) \propto e^{-\beta U(\mathbf{x}^{3N}, \sigma^N)} \tag{3.13}$$

An efficient Metropolis sampling in this ensemble consists of two types of trial moves with subindex o for old and n for new configuration: (i) particle displacement $\mathbf{x}_o^{3N} \to \mathbf{x}_n^{3N}$, e.g. interchanging two random atoms or (ii) compositional change $\sigma_o^N \to \sigma_n^N$, e.g. changing the spin on one random site. The acceptance likelihood of these trial moves is then (with U computed using a suitable Hamiltonian)

$$\mathcal{A}_C = \min\left\{1, e^{-\beta\Delta U}\right\} \tag{3.14}$$

$$\Delta U = U(\mathbf{x}_n^{3N}, \sigma_n^N) - U(\mathbf{x}_o^{3N}, \sigma_o^N) \tag{3.15}$$

3.3.2 Semi-Grand Canonical Ensemble

The partition function of the semi-grand canonical (SGC) ensemble can be expressed in terms of the canonical partition function Z_C as

$$\mathcal{Z}_S(\Delta\mu, \mathcal{N}) = \int \mathcal{Z}_C(c, \mathcal{N}) e^{-\beta\Delta\mu N c}\, \mathrm{d}c \tag{3.16}$$

The corresponding probability distribution is thus

$$\mathcal{P}_S(\mathbf{x}^{3N}, \sigma^N; \Delta\mu, \mathcal{N}) \propto e^{-\beta\left[U(\mathbf{x}^{3N}, \sigma^N) + \Delta\mu N c\right]} \tag{3.17}$$

which implies an acceptance probability of

$$\mathcal{A}_S = \min\left\{1, e^{-\beta[\Delta U + \Delta\mu N \Delta c]}\right\} \tag{3.18}$$

with ΔU defined above. The trial moves in the SGC ensemble consist of, apart from the trial moves mentioned for the canonical ensemble also the possibility of a change of species. In practise the particle displacement trial move, i.e. the interchanging two random atoms, is replaced by the change of species trial move, i.e. the species of a random atom is changed.

A most useful relationship that is derived in section A.4 is

$$\Delta\mu(c) = -\frac{1}{N}\left(\frac{\partial F_C}{\partial c}\right)_{V,T} \tag{3.19}$$

The extent of its usefulness will be made clear in section 5 but also its shortcomings.

3.3.3 Variance Constrained Semi-Grand Canonical Ensemble

Due to the fact that the second derivative of the free energy is negative inside the miscibility gap the relation (3.19) is not a one-to-one function and knowledge of $\Delta\mu$ is not enough to determine c and through integration obtain the free energy F. These shortcomings can be

remedied by the variance constrained semi-grand canonical (VC-SGC) ensemble which can be defined, in terms of the canonical ensemble, through the partition function as

$$\mathcal{Z}_V(\phi,\kappa,\mathcal{N}) = \int Z_C(c,\mathcal{N}) e^{-\beta N c\,(\phi+\kappa N c)}\,\mathrm{d}c \tag{3.20}$$

where ϕ and κ are independent Lagrangian multipliers defining the constraint on the concentration. The derivation of this relation is beyond the scope of the present text but can be found in [18]. The corresponding probability density for the VC-SGC ensemble is then

$$\mathcal{P}_V(\mathbf{x}^{3N},\sigma^N;\phi,\kappa,\mathcal{N}) \propto e^{-\beta U(\mathbf{x}^{3N},\sigma^N)} \cdot e^{-\beta N c(\phi+\kappa N c)} \tag{3.21}$$

The VC-SGC ensemble can be regarded as a generalisation of the SGC and canonical ensembles. The former can be obtained by letting $\kappa \to 0$ and identifying ϕ with $\Delta\mu$. The latter can be obtained by first completing the square and rewriting (3.21) as

$$\mathcal{P}_V \propto e^{-\beta U} \cdot e^{-\beta N c(\phi+\kappa N c)} \propto e^{-\beta U} \cdot e^{-\beta\kappa(Nc+\frac{\phi}{2\kappa})^2} \tag{3.22}$$

and then letting $\kappa, \phi \to \infty$ while keeping the ratio $\phi/\kappa = -2Nc$. What one thus obtains is basically equation (3.20) with the exponential replaced with a delta function that keeps the concentration constant. The VC-SGC ensemble is thus a generalisation of the canonical ensemble with the delta function replaced with a Gaussian with adjustable width determined by the parameter κ.

Due to the similarity of the VC-SCG to the canonical ensemble an efficient Metropolis algorithm is easily formulated in analogy with the previous section, where a trial move consists of selecting a random site, performing either a compositional change $\sigma_o^N \to \sigma_n^N$ or a particle displacement $\mathbf{x}_o^{3N} \to \mathbf{x}_n^{3N}$, computing the change in energy ΔU, concentration $\Delta c = c_n - c_o$ as well as $\tilde{c} = \frac{1}{2}(c_n + c_o)$. The acceptance likelihood for the trial move is

$$\mathcal{A}_V = \min\left\{1, e^{-\beta[\Delta U + N\Delta c(\phi+2\kappa N\tilde{c})]}\right\} \tag{3.23}$$

The energy change associated with the trial move thus gets two contributions, one from the change in the interatomic potential ΔU and one from concentration dependent force described by the harmonic potential $N\Delta c(\phi + 2\kappa N\tilde{c})$. To see that this is in fact a harmonic potential refer to equation (3.22). The advantage of this additional concentration dependent potential is readily seen in figures 5.1 in section 5.2.1 where the SGC cannot sample the free energy inside the miscibility gap, where the second derivative of the free energy is negative, whereas the VC-SGC can due to the fact that we can constrain the sampling to within a certain region in concentration space.

When ensemble averaged, the equilibrium chemical driving force which correspond to the $\Delta\mu$ parameter in the SGC ensemble becomes

$$-\frac{\partial F}{\partial c} = \phi + 2\kappa N \langle c \rangle_V \tag{3.24}$$

This very important relation, the derivation of which can be found in [18], allows us to sample the free energy inside the miscibility gap.

3.3.4 Interface Free Energy in Simulations

The free energy obtained in this work does not correspond to a random solution since the trial moves in a VC-SGC ensemble together with the detailed balance criterion are designed to produce the most likely configurations of the solution. The volume term Δg_v from equation (2.2) is still the driving force, but since decomposition is allowed to occur this term Δg_v is effectively taken out of the equation. Furthermore, no misfit strain is possible in the lattice model used and the misfit term $\Delta g_s = 0$. Neglecting of volume change also implies that $\Delta F = \Delta G$. What remains of equation (2.2) is then

$$\Delta F = A\gamma \tag{3.25}$$

In order to obtain a precise value of γ the shape of the precipitate and direction of the interface is important. If the variation of γ with direction is neglected for the moment it is obvious that the precipitate will take the form which minimises the ratio between interface area and precipitate volume, i.e. the sphere. When the concentration increases the volume of the precipitate increases. When the diameter of the spherical precipitate equals the size of the (cubic) system L the interface area will be $4\pi r^2 = 4\pi(L/2)^2 = \pi L^2$. However, due to periodic boundary conditions, the sphere is then no longer the shape with the smallest interface area since a flat interface will have an area of $2L^2$. A further increase in concentration will then only move the interface in the direction perpendicular to the interface and the interface area will remain constant until the point is reached where the precipitate and the matrix interchange functions.

Since γ is different in different directions it is desirable to constrain the interface to only flat interfaces in order to facilitate calculations. One way to achieve flat interfaces is to run the simulation in a system of size $L_x = L_y < L_z$ as shown in Figure 3.1. The interface will then form perpendicular to the z-direction and the interface area will be $A = 2L_xL_y$. The quantity obtained in the simulations $\Delta F/N$ is the free energy per atom where, since a bcc structure with two atoms per unit cell is assumed, $N = 2 \cdot L_xL_yL_z$. The interface free energy per unit volume Δf is then

$$\frac{\Delta f}{2} = \frac{\Delta F}{N} = \frac{A\gamma}{2L_xL_yL_z} = \frac{2L_xL_y\gamma}{2L_xL_yL_z} = \frac{\gamma}{L_z} \tag{3.26}$$

and a plot of $\Delta F/N$ vs. $1/L_z$ would yield a straight line, where γ is the slope. Note also that the interface free energy per unit volume will go to zero when the system size goes to infinity. This can be understood intuitively since the ratio of the interface area over the volume of the precipitate which will go as $1/L$.

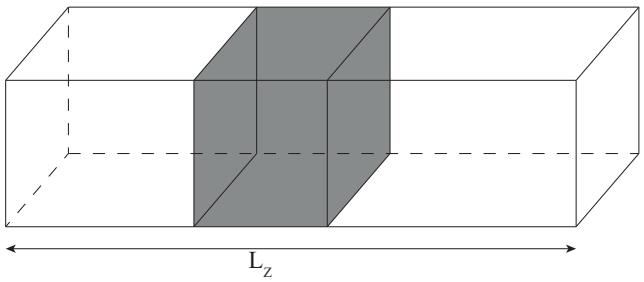

Figure 3.1: *Illustration of a flat interface*

4 Order Parameters

4.1 Definition of Order Parameters

A phase diagram is a map of which phases of properties a system has under different system parameters. Often the system parameter on the abscissa is the concentration and on the ordinate the temperature. The boundaries in the phase diagram show equilibrium between different phases.[1] On the boundary between two phases small changes in the system parameters lead to big changes in order parameters. If the order parameters are being recorded throughout the sampling, the mean value will give a measure of the type of order, a measure that will change rather abruptly at the phase boundary. Since the sampling process at or near the phase boundaries samples states which alternate between the sides of the phase boundary the variance defined as $\sigma^2 = \langle E^2 \rangle - \langle E \rangle^2$ will peak at the phase boundary. The quantity σ, which is the square root of the variance, is referred to as the standard deviation.[2] There are two main groups of order parameters used to characterise the phases, short range order (SRO) parameters and system averages. The magnetisation is an example of the latter kind.

4.1.1 Critical Temperatures

The magnetisation is computed as

$$M = \frac{1}{N} \sum_{i=1}^{N} \sigma_i \tag{4.1}$$

and $\langle M \rangle$ is the magnetisation during the course of the simulation, see equation (3.7). A characteristic feature of a ferromagnetic material is that there is a net magnetisation for low temperatures while at higher temperatures the net magnetisation disappears and the material becomes paramagnetic. The critical temperature at which this happens is called the *Curie temperature*. For iron the Curie temperature is 1043 K.

While iron is ferromagnetic chromium is antiferromagnetic, meaning that there is no net magnetisation. In contrast to a paramagnetic state there is order in the material, the magnetic moments are aligned antiparallel. The critical temperature at which the antiferromagnetic order disappears is called the *Néel temperature*. The Néel temperature for chromium is 308 K. Since neither an antiferromagnetic material nor a paramagnetic material has a net magnetisation there is no discontinuity of the mean magnetisation at the critical temperature and the magnetisation cannot be used as the order parameter to study phase transitions between antiferromagnetic and paramagnetic regions. However, since antiferromagnetic material possesses short range order (the magnetic moments are antiparallel) while the paramagnetic does not (the order is random) the transition can be studied through short range order parameters.

[1] Phase diagrams are discussed in appendix B

[2] Due to the close relation between the variance and the standard deviation both are in this work referred to as the fluctuations.

4.1.2 Short Range Order Parameters

Short range order (SRO) can be studied through the Warren-Cowley [19] or atomic SRO parameter (ASRO) defined as

$$\alpha_A^{(i)} = 1 - \frac{Z_{Fe}}{Z_{tot}(1 - c_{Cr})} \tag{4.2}$$

where Z_{Fe} is the number of iron neighbours of a studied chromium atom, Z_{tot} is the total number of neighbours and c_{Cr} is the total concentration of chromium in the material.

For low concentrations chromium will mix with Fe leading to $Z_{Fe} \approx Z_{tot}$ which leads to $\alpha = -c/(1-c) < 0$ where we have dropped the indices for simplicity. For very high concentrations of chromium $Z_{Fe} \to 0$ while $(1 - c) \to 0$, but since we can write $Z_{Fe} \approx Z_{tot}(1 - c)$ we have

$$\alpha_A^{(i)} = 1 - \frac{Z_{Fe}}{Z_{tot}(1 - c)} \approx 1 - \frac{Z_{tot}(1 - c)}{Z_{tot}(1 - c)} = 0 \tag{4.3}$$

However, equation (4.3) is in fact more general and $\alpha = 0$ whenever the expected number of chromium neighbours consistent with the concentration c are encountered. Values of $\alpha^{(i)} > -c/(1 - c)$ and positive values in particular are found when there is an over representation of chromium neighbours, i.e. when chromium forms clusters or precipitates. The sign of $\alpha^{(i)}$ will thus tell us if chromium mixes with iron or precipitates. The absolute value will tell us to what extent this happens.

One can also define a magnetic SRO-parameter (MSRO) in analogy with (4.2) which measures not the atomic ordering but the ordering of the magnetic moments.

$$\alpha_M^{(i)} = 1 - \frac{\sigma_\pm}{\sigma_{tot}\frac{1}{2}(1 \pm M)} \tag{4.4}$$

where $\sigma_\pm$ is the number of neighbours with parallel spins[3], σ_{tot} is the total number neighbours and $\sigma_{tot}\frac{1}{2}(1 \pm M)$ is the expected number of neighbours with parallel spins.[4] Thus if the total magnetisation is zero $\alpha_M = 0$ if there is no order and positive if there is order. In a perfect antiferromagnetic state we can expect $\alpha_M = 6/14$.[5]

Note that $\alpha^{(i)}$ is a local parameter and the SRO-parameter for the lattice as a whole is the average of all local $\alpha^{(i)}$ over all sites; in the case of the ASRO, all the chromium atoms and in the case of the MSRO all atoms with parallel spin so that

$$\alpha_A = \frac{1}{\#\text{Cr}} \sum_{\text{Cr}} \alpha_A^{(i)} \quad \text{and} \quad \alpha_M = \frac{1}{\#\text{atoms}} \sum_{\text{atoms}} \alpha_M^{(i)} \tag{4.5}$$

[3] If the atom of study has spin up, σ_+ is the number of spin up, and consequently if the atom of study has spin down, σ_- is the number of spin down. The sign in the denominator corresponds to a similar index of σ.

[4] For example, if $M = 1$ only spin up (σ_+) is allowed and the denominator takes the value of σ_{tot} which is consistent with all spins being parallel while if $M = 0$ the denominator is $\frac{1}{2}\sigma_{tot}$ which means that half of the spins are parallel and the other half antiparallel.

[5] This can be seen from the antiferromagnetic configuration in section D.2.

4.1.3 Total Energy

The fourth quantity measured during the simulations, the total energy, does not provide any new information about the system that is not already included in the previously mentioned order parameters, but it does provide a qualitative understanding of the nature of the phase transitions in addition to being a cross correlation reference. The total energy, often denoted U, is the ensemble average of E so that U can be expressed through the well-known thermodynamic relation

$$U = \langle E \rangle = \frac{\sum_s E_s e^{-\beta E_s}}{\sum_s e^{-\beta E_s}} = -\frac{\partial}{\partial \beta} \ln Z \tag{4.6}$$

where Z is the partition function. Through straight-forward differentiation one obtains

$$C_V = \left(\frac{\partial U}{\partial T} \right) = -\frac{\partial \beta}{\partial T} \frac{\partial^2}{\partial \beta^2} \ln Z = \frac{1}{k_B T^2} \left(\left\langle E^2 \right\rangle - \langle E \rangle^2 \right) = \frac{\sigma_E^2}{k_B T^2} \tag{4.7}$$

The heat capacity is thus proportional to the square of the standard deviation and the shape of the graphs of the energy and the fluctuations of the energy will tell us what type of transition there are, e.g. since the Curie temperature is a second order phase transition we can expect a lambda type graph of the standard deviation. It is also apparent that the method of studying the standard deviations for obtaining the phase boundaries used in this work is equivalent to studying the heat capacity of a system.

4.1.4 Mean and Standard Deviation

During a simulation the quantities recorded after each Monte Carlo step were; the energy (E), the magnetisation (M), the atomic SRO parameter (α_A) and the magnetic SRO parameter (α_M) as well as acceptance probabilities, i.e. the number of accepted trial moves compared to the total number of trial moves. After completing a simulation the average value $\langle A \rangle$ and the standard deviation σ_A (indexed A for which parameter the standard deviation is taken) are computed respectively as

$$\langle A \rangle = \frac{1}{M_C} \sum_{i=1}^{M_C} A_i \tag{4.8}$$

$$\sigma^2 = \left\langle A^2 \right\rangle - \langle A \rangle^2 = \frac{1}{M_C} \sum_{i=1}^{M_C} A_i^2 - \left(\frac{1}{M_C} \sum_{i=1}^{M_C} A_i \right)^2 \tag{4.9}$$

where A_i is the value recorded after each MC step and M_C is the number of MC steps. If the mean value is a thermodynamic quantity the standard deviation is closely related to the derivative of that quantity, e.g. the standard deviation of the total energy is closely related to the heat capacity.

4.1.5 Details of simulations

Monte Carlo simulations were carried out on an Fe-Cr alloy using the Metropolis algorithm for the modified Ising model described in section 3.1.1. Since both iron and chromium form

a bcc-lattice at moderate temperatures with almost the same lattice parameter (2.87 Å for Fe and 2.88 Å for Cr [15]), the code was written under the assumption that the alloy forms a bcc-structure with a common lattice parameter set to unity. The magnetic interactions described by the Ising model were assumed to extend with the same magnitude to first and second neighbours making the total number of interacting neighbours 14. Since the atoms on the boundary have no neighbours and this would create an unwanted interface periodic boundary conditions were used.

The simulations were carried out in a 20^3 bcc supercell with periodic boundary conditions using a canonical ensemble with a fixed temperature and concentration[6] with trial moves of either (i) a random displacement, i.e. two random atoms changing places, or (ii) a spin flip, the spin of a random site is changed. The fraction of atom swaps were the same as the concentration of the minority species. Initially the averaging was performed over 25000 MC steps but to improve accuracy some figures are averaged over 1000 MC steps after a gradual decrease of temperature had put the system in an equilibrium configuration.

During the simulation the values of the energy, magnetisation and the SRO parameters α_A defined in equation (4.2) and α_M defined in equation (4.4) were recorded after each MC step. The average values and standard deviations were computed after a rejection of the first non-equilibrium configurations. The phase diagram for Fe-Cr was obtained through the analysis of these three different order parameters, the magnetisation M, the two SRO-parameters α_M and α_A and was cross correlated with the values obtained for the total energy.

4.1.6 Construction of Phase Diagram

The Curie temperature, the temperature at which the total magnetisation disappear, is a second order phase transition and was taken as the point at which the standard deviation peaked.

The Néel temperature cannot be obtained so easily since both the antiferromagnetic region below the Néel temperature and the paramagnetic temperature above have a net magnetisation equal to zero. However, the magnetic short range order parameter (MSRO) defined in section 4.1.2 takes a value of 6/14 for an antiferromagnetic material and zero for paramagnetic.[7] The Néel temperature was taken as the point at which the standard deviation of the MSRO peaked.

The Miscibility gap was generated through the atomic SRO-parameter (ASRO). After each MC step the ASRO was recorded and the mean value was taken as the thermal equilibrium value. The value of the system parameters that caused the standard deviation to peak was taken as the boundary for the miscibility gap. The values for the ASRO as a function of concentration were cross correlated with the values of the ASRO as a function of temperature. From the simulations at each temperature two points were generated for the boundary of the miscibility gap, one for the α-phase (solution of chromium in iron base) and for α'-phase (solution of iron in chromium base).

[6] The simulations in a canonical ensemble can be regarded as semi-grand canonical ensemble simulations but since the concentration is not allowed to vary and only relative probabilities can be computed, the concentration factor only contributes with a multiplicative constant which cancels.

[7] See section D.2 for a discussion on antiferromagnetic configurations.

4.2 Results

4.2.1 Acceptance Probabilities

Figure 4.1a shows the number of accepted trial moves divided by the total number of trial moves for $\Delta U > 0$ as a function of temperature for different concentrations. The non-trivial behaviour of the acceptance probability $\mathcal{A}_C = \min\left\{1, e^{-\beta\Delta U}\right\}$ is due to the fact that not only does the acceptance probability depend explicitly on the temperature but also implicitly through ΔU, where ΔU is the energy difference between the old and the new configuration.

The acceptance probability increases with concentration due to the decrease in ΔU associated with a trial move. This can be understood from the higher multiplicity of a state at higher concentration, i.e. at low concentrations the mean spin is high and all spins are aligned parallel. A trial move consisting of a spin flip would then result in a high ΔU causing a low acceptance probability.

The low acceptance probability for low temperatures is important. Specially, the acceptance probability is less than 0.01 for some concentration for temperatures below $T = 2$. As a consequence the time for the system to reach equilibrium at low temperatures is long. This can be seen from Figure 4.1b which shows the total energy as a function of the number of MC steps at different temperatures. The noise is due to thermal fluctuation around the average value, the thermodynamic state.

Another consequence of the low acceptance probability at low temperatures is that the probability for the system to move from one local minimum to another is negligible since the thermal energy is not enough to overcome the threshold barrier and even though a stable average is reached there is no guarantee that the sampled state is the global minimum.

4.2.2 Magnetisation

Figure 4.2a shows the temperature dependence of the magnetisation for concentrations up to an atomic fraction of 0.7 Cr. The graph shows a clear second order phase transition from ferromagnetic to paramagnetic.

For low values of c, up to $c < 0.25$, the chromium atoms are soluble in the iron and there is a $1 - 2c$ dependence on the magnetisation. This happens because for every chromium atom the total spin reduces with 2σ; firstly because one iron atom is missing and the secondly because it is replaced by a chromium atom which is aligned antiparallel.

For $c = 0.3$ a slight and unexpected increase in magnetisation with temperature can be seen. Ackland [11] attributes this to formations of small clusters of Cr in ferromagnetic regions by thermal fluctuation despite being energetically unfavourable. This behaviour would be difficult to measure experimentally since a Curie temperature for pure iron of 11.8 in reduced units corresponds to 1043 K, the reduced temperature 2.5 would correspond to 220 K, a temperature at which thermal equilibrium is difficult to achieve in practise due to the low diffusion rate.

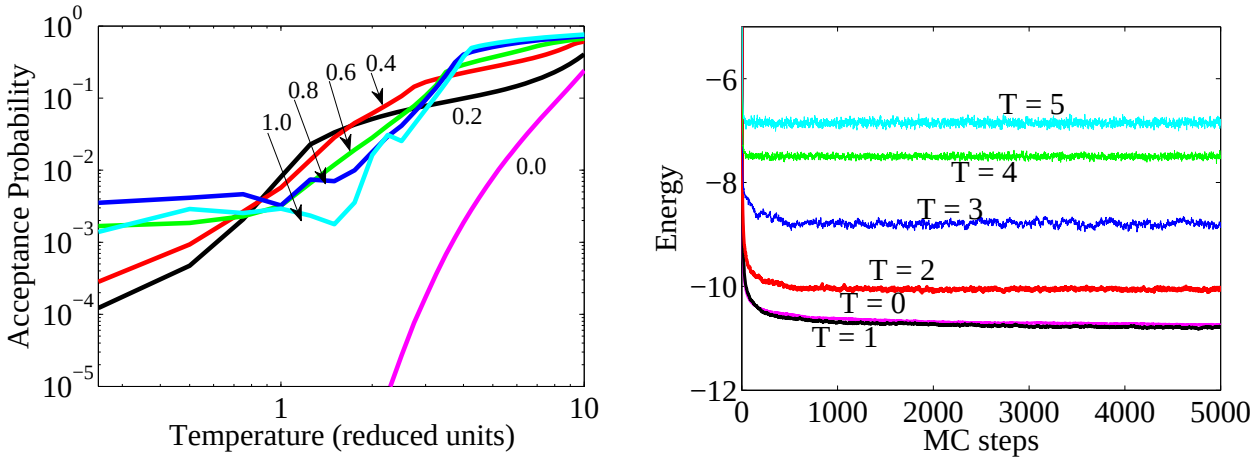

(a) (b)

Figure 4.1: (a) *Acceptance probability as a function of temperature for different concentrations. Note the logarithmic scales. For low temperatures the acceptance probability is very small and good statistics is difficult to obtain.* (b) *The total energy at different temperatures plotted versus the number of MC steps for a* 20^3 *bcc supercell at concentration 0.5.*

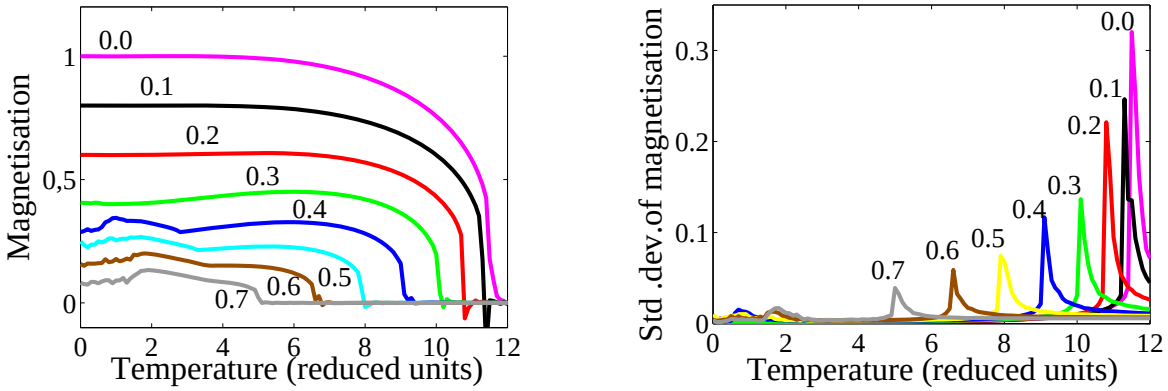

(a) (b)

Figure 4.2: *Magnetisation* (a) *and standard deviation of magnetisation* (b) *as a function of temperature averaged over 25000 MC-steps. Results were obtained from a bcc crystal with* 20^3 *unit cells. Note the distinctive* λ*-type phase transition which makes determination of the Curie temperature straight-forward.*

A similar behaviour is seen also for $c = 0.4$ and 0.5 above a pronounced minimum at a particular temperature which increases with temperature. This minimum corresponds to the miscibility gap inside which chromium rich precipitates form an antiferromagnetic structure which increases the total magnetisation.

Also for $c = 0.6$ and 0.7 there is a clear dent in the graph although not a minimum. Above $c = 0.7$ magnetisation can only occur below the temperature at which iron-rich precipitates form in the otherwise chromium rich base.

Figure 4.2b shows the standard deviation of the magnetisation. The second order nature of the phase transition at the critical temperature is here obvious. One observes that not only does the temperature at which the standard deviation reaches a maximum decrease but also the value at the maximum decreases with increasing amount of chromium just as the magnetisation itself decreases making the critical temperature less pronounced. For higher concentrations there is also a pronounced wiggliness for low temperatures in figure 4.2a. This may have two reasons, for low temperatures the Boltzmann factor goes to 0 and the acceptance probability for $\Delta U > 0$ goes to 0. Thermal equilibrium would thus require a much longer time to accomplish than the 25000 MC steps used here and detailed balance is not satisfied. But since the wiggliness is only pronounced inside the miscibility gap the fluctuations may be caused by formation of precipitates of different sizes by thermal fluctuations

4.2.3 Magnetic Short Range Order Parameter

The temperature dependence of the magnetic moment short range order parameter α_M for some different concentrations can be seen in Figure 4.3a and the corresponding standard deviation in Figure 4.3b. It can be seen in Figure 4.3a that for pure chromium the MSRO reaches a maximum value of 6/14 that is consistent with the theoretical maximum value for an antiferromagnetic structure. The noise in the graph for $c = 0.9$ below $T = 2$ is most likely caused by the formation of precipitates and disappears above the miscibility gap. It also appears that one can see the transition between miscibility gap and the antiferromagnetic region for $c = 0.9$ at a temperature $T = 2$.

Figure 4.3b shows that, similarly to the Curie temperature, the Néel temperature is a second order phase transition and the critical temperature is easily determined from the peaks in the fluctuation of the MSRO. The Néel temperature reaches a maximum value for pure chromium and decreases slightly with decreasing chromium content which is consistent with the usual behaviour of alloys, where impurities tend to destroy the order and increase the entropy thus lowering the phase transition temperature compared to the pure substance.

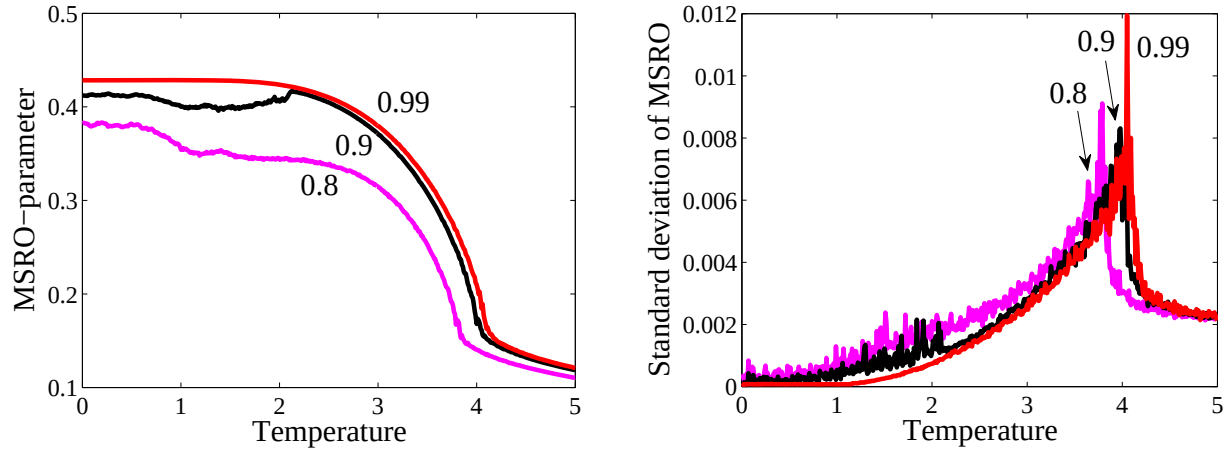

(a) (b)

Figure 4.3: *Magnetic SRO-parameter* (a) *and standard deviation of magnetic SRO-parameter* (b) *as a function of temperature at different concentration averaged over 1000 MC steps where the starting configuration was generated through a gradual decrease of temperature of* $\mathrm{d}T = 0.01$ *from the previous configuration.*

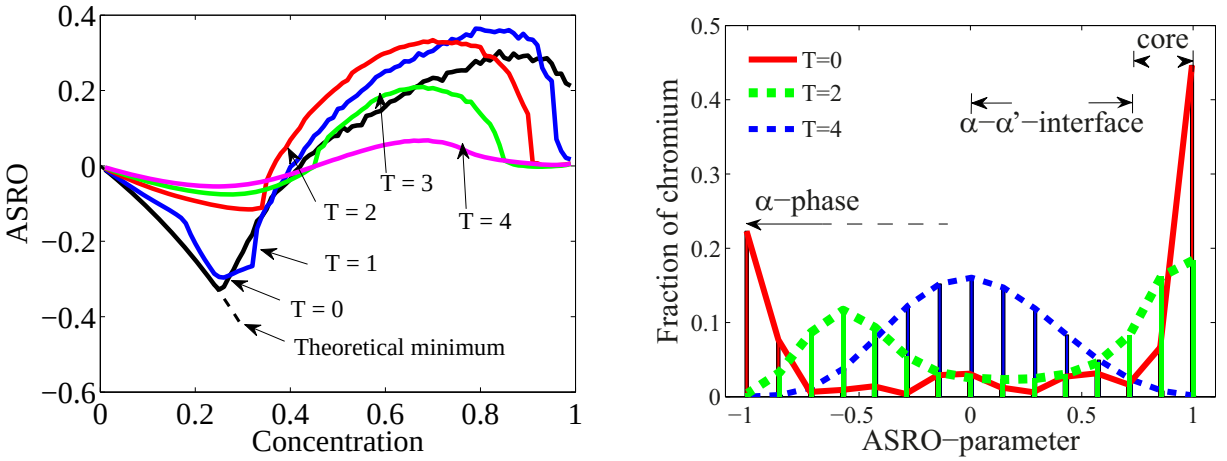

(a) (b)

Figure 4.4: *ASRO-parameter as a function of concentration at different temperatures* (a) *averaged over 1000 MC steps where the starting configuration was generated through a gradual decrease of temperature of* $\mathrm{d}T = 0.01$ *from the previous configuration. The relative distribution of the ASRO parameter for* $c = 0.5$ *at different temperatures* (b) *averaged over 10 000 MC steps.*

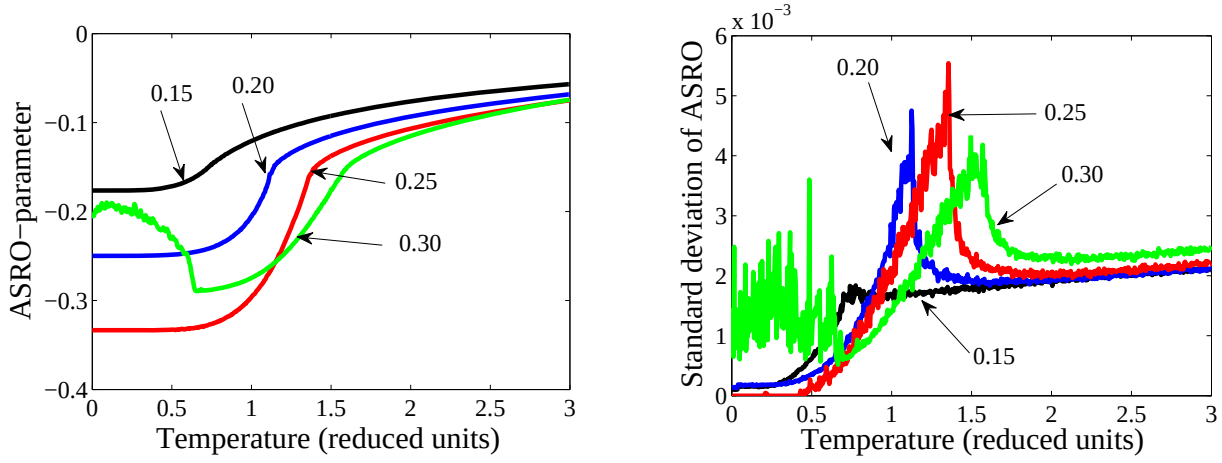

(a) (b)

Figure 4.5: *ASRO-parameter as a function of temperature at different concentrations* (a) *the corresponding standard deviation* (b)*. The values were averaged over 1000 MC steps where the starting configuration was generated through a gradual decrease of temperature of* $\mathrm{d}T = 0.01$ *from the previous configuration.*

4.2.4 Atomic Short Range Order Parameter

Figure 4.4a shows the atomic SRO-parameter as a function of concentraion. The theoretical minimum value of the ASRO parameter in is given by $\alpha_A = -c/(1-c)$ for a perfect solution of chromium in iron and one can see that $T = 0$ initially follows the theoretical minimum since there are no thermal fluctuations.[8]

After an initial decrease of the ASRO-parameter the graph displays an increase associated with the formation of precipitates. For temperature $T = 2$ this transition is particularly pronounced. For $T = 4$ the ASRO in Figure 4.4a is close to zero regardless of concentration. This implies that no precipitates form since the thermal fluctuations cause clusters to dissolve immediately upon formation and that the miscibility gap does not extend up to $T = 4$. This is also confirmed by Figure 4.4b, which shows the relative distribution of the ASRO for a chromium concentration of 0.5 at different temperatures. It can be seen that for temperature $T = 4$ the distribution of the ASRO-parameter exhibits a clear gaussian shape around zero, whereas for temperatures $T = 0$ and $T = 2$ the chromium atoms appear either as clusters with $\alpha_A \approx 1$ or in solution with $\alpha_A \approx -1$. The small peak for mid-range ASRO corresponds to an interface.

For $T = 1$ in Figure 4.4a there are two changes in direction before the onset of precipitation. In Figure 4.8a the reason for this becomes apparent. An area of high fluctuations of the ASRO parameter between the points $c = 0.2$ and $T = 1$ to $c = 0.3$ and $T = 1.5$ is seen. From

[8]Some careful analysis shows that the maximum concentration at which the theoretical minimum can be reached is $c = 0.25$, which is the highest concentration where no two chromium atoms are first or second nearest neighbour. One configuration that satisfies this is two chessboard layers on top of each other, shifted such that iron is always above chromium and vice versa, interlaced with a pure iron layer.

Figure 4.5a, which show the ASRO as a function of temperature for fixed concentrations, and particularily from Figure 4.5b, which shows the corresponding standard deviation, it can be deduced that there is an additional phase transition. The continuous behaviour of Figure 4.5a and the lambda type appearence of Figure 4.5b confirms that this is a second order phase transition.

For $c = 0.30$ the erratic behaviour below $T = 0.7$ in both Figures 4.5a and 4.5b is caused by precipitation and marks the boundary of the miscibility gap. It is thus obvious that this phase transition is in no way related to the border of the miscibility gap.

4.2.5 Energy

Figure 4.6a shows the temperature dependence of the energy of the Fe-Cr system for atomic chromium fractions of 0.0, 0.2, 0.4, 0.6, 0.8 and 1.0. Just as in the case of the magnetisation one can see clear tendencies to a second order phase transition consistent with the Curie Temperature. The Curie temperature manifests itself as a notch above which the graph flattens out. As expected this notch appears at lower temperature for higher concentrations.

One also notices a second transition in the graph which moves towards higher temperatures and becomes more pronounced for higher concentrations. This transition is due to precipitates which appear below thus lowering the energy and marks the transition from the two phase region to the α-phase. For $c = 0.8$ the miscibility gap extends into the paramagnetic region which can be seen as the two transitions melting together.

The standard deviation, which is closely related to the heat capacity[9], is seen in Figure 4.6b The lambda type transition is here obvious. The Curie temperature is seen as a peak in the standard deviation which is not necessarily the maximum value. The precipitates are also seen quite clearly as high values in Figure 4.6b.

Figure 4.8b shows a plot of the fluctuations of the energy as a function of both temperature and concentration. The points of high fluctuations form ridges corresponding to the critical temperatures for ferromagnetic and antiferromagnetic phase as well as the upper temperature boundary of the miscibility gap.

4.2.6 The Heusler Phase

Figure 4.7 shows the configurations of $c = 0.25$ at $T = 0$ and $T = 3$ respectively. The second order phase transition mentioned above is thus a transition from ordered to disordered structures. The configuration of Figure 4.7a consists of two chessboard layers on top of each other, shifted such that iron is always above chromium and vice versa, interlaced with a pure iron layer. A unit cell for this structure is shown in Figure 4.7c. The *Strukturbericht* is $L2_1$ and the Space Group is $Fm\bar{3}m$. The structure resembles the ternary Heusler alloy and we will call this phase the Heusler phase and denote it η-phase.

[9] See equation (4.7)

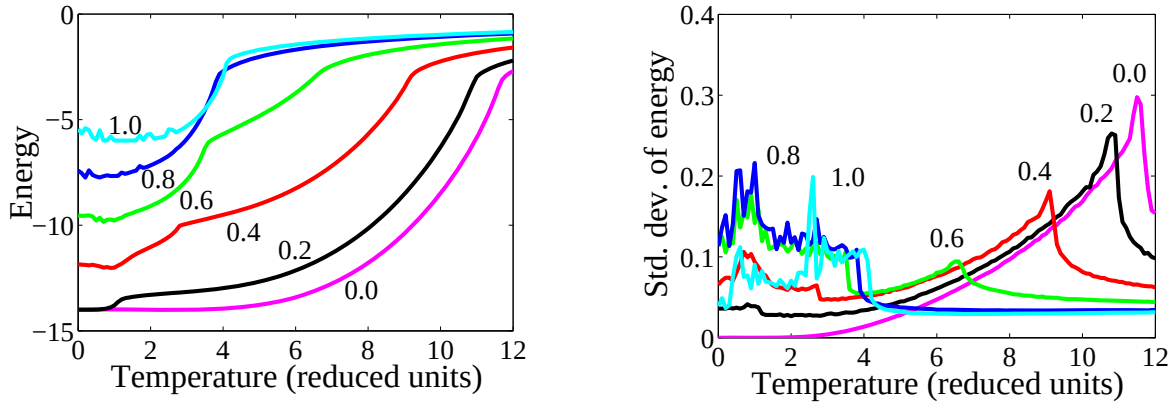

(a) (b)

Figure 4.6: (a) *Average energy per atom as a function of temperature averaged over 25000 MC steps. For concentration 0.4 and 0.6 there are two notches which correspond to phase transitions, first at higher temperature because of the transition from ferromagnetic phase to paramagnetic and secondly at a lower temperature because of precipitation. For concentrations 0.0 and 0.2 there is only one transition, from ferromagnetic to paramagnetic and for 0.8 the two notches coincide at the same temperature.* (b) *Standard deviation of energy as a function of temperature which is closely related to the heat capacity (see section 4.2.5).*

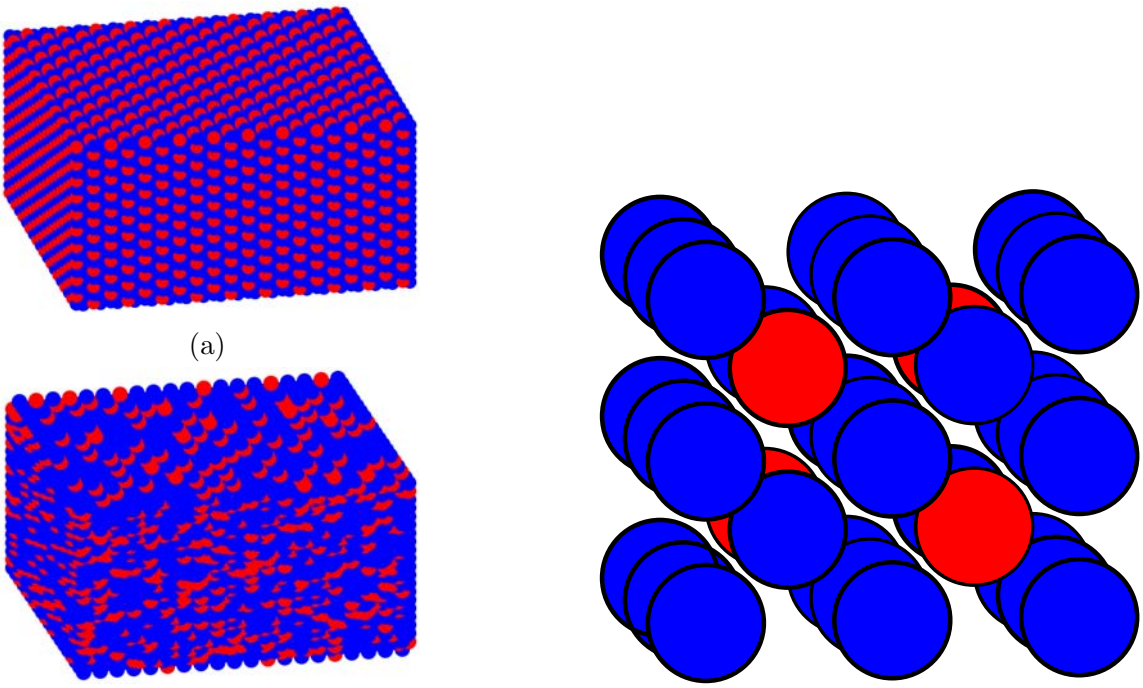

(a)

(b) (c)

Figure 4.7: (a) *Ordered Heusler-phase (η) at $c = 0.25, T = 0$ and* (b) *Disordered α-phase at $c = 0.25, T = 3$.* (c) *Unit cell of the Heusler-phase which consists of 2x2x2 conventional bcc unit cells where the middle atom is alternating chromium and iron. The blue dots represent iron atoms and the red represent chromium.*

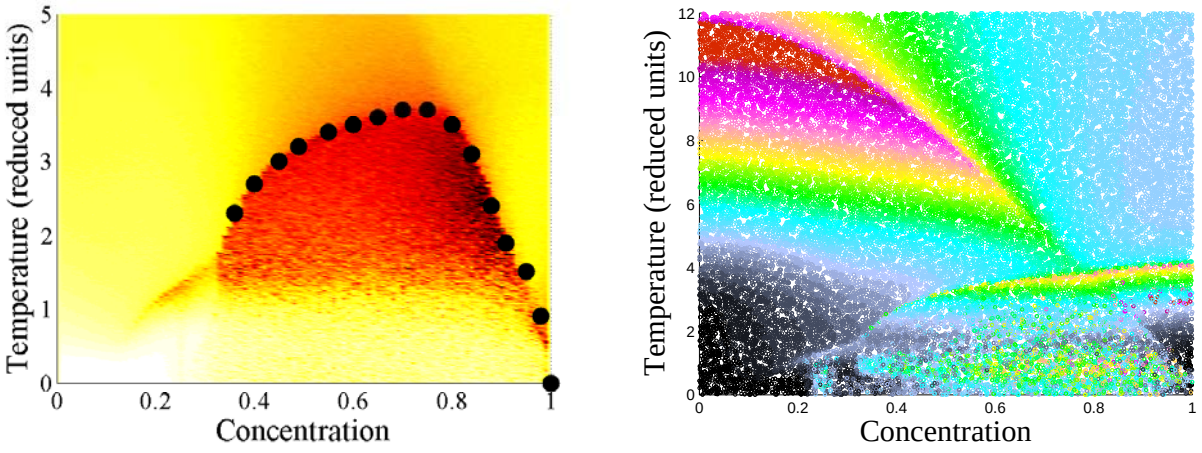

(a) (b)

Figure 4.8: (a) *ASRO-parameter as a function of both concentration and temperature averaged over 1000 MC steps.* (b) *Standard deviation of the energy as a function of temperature and concentration averaged over 10 000 MC steps.*

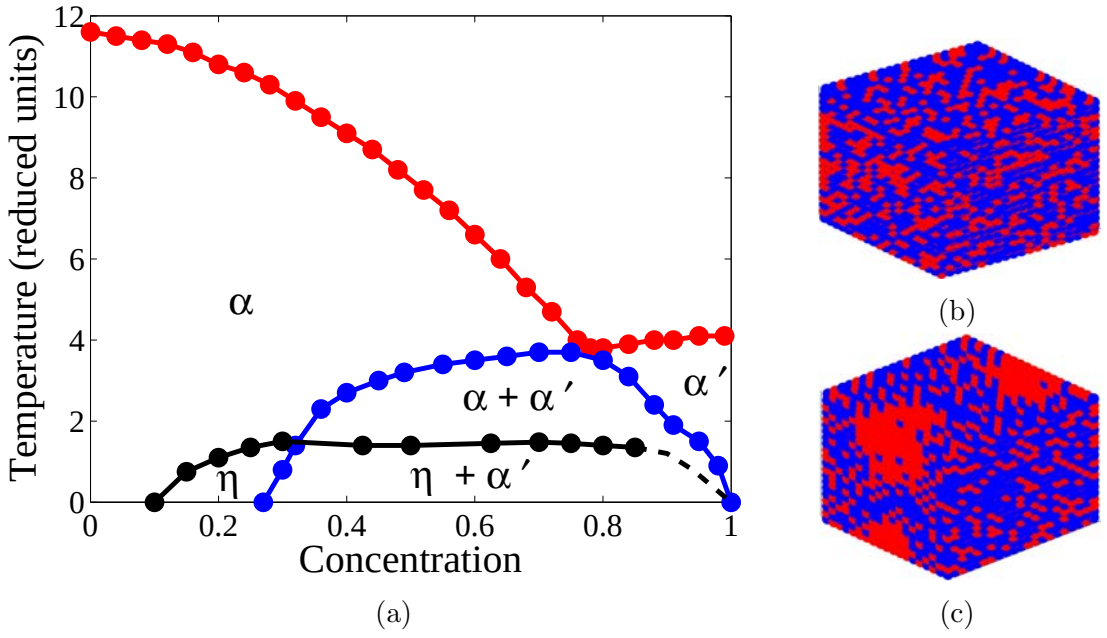

(a) (b) (c)

Figure 4.9: *(a) Phase diagram of Fe-Cr computed using a modified Ising model in a* 20^3 *bcc lattice with second nearest neighbours interaction. (b) Solution of* α*-phase* $c = 0.4, T = 4$*. (c) Precipitation of* $\alpha + \alpha'$ *inside the miscibility gap* $c = 0.4, T = 2$*. The blue dots represent iron atoms and the red represent chromium.*

4.2.7 Phase Diagram

Combining all the data generated through the order parameter analysis yields the phase diagram in Figure 4.9a. The Curie temperature was found using the magnetisation order parameter, the Néel temperature from the magnetic SRO parameter and the miscibility gap as well as the Heusler phase was found using the atomic SRO parameter. The data were cross correlated between the order parameter as a function of concentration and the order parameter as a function of temperature. All data points were also cross correlated with data for the total energy.

The phase diagram shows three qualitatively different phase boundaries, the critical temperature boundary for the ferromagnetic and antiferromagnetic phases, the boundaries between the miscibility gap, iron-rich α-phase or the chromium-rich α'-phase respectively, and the boundary between ordered η-phase and disordered α-phase.

5 Free Energy

5.1 Obtaining the Interface Free Energy

Simulations of a Semi-Grand Canonical (SGC) ensemble or a Variance Constrained Semi-Grand Canonical (VC-SGC) ensemble consist of two different types of trial moves, either (i) a spin flip, the spin of a random site is changed or (ii) element swap, the atom type is swapped from Fe to Cr or vice versa[18]. The ratio between the different trial moves were equal fractions. For each chosen value of the SGC parameter $\Delta\mu$ the concentration was calculated as the average value of the concentration after each iteration $\langle c \rangle$.

The simulation of the free energy in the SGC ensemble suffers from some shortcomings which will be discussed below. The free energy inside the miscibility gap cannot be obtained via simulations in the SGC ensemble. These shortcomings can be remedied by the Variance Constrained Semi-Grand Canonical (VC-SGC) ensemble.

In order to constrain the concentration and obtain a one-to-one relation between $\partial F/\partial c$ and concentration the VC-SGC parameter κ was chosen[1] to $1/N$, where N is the number of atoms in the system, and through the relation

$$\Delta\mu = \phi + 2\kappa N \langle c \rangle_V \tag{3.24}$$

the derivative of the free energy was obtained from which the free energy F was calculated through numerical integration using the trapezoidal rule and relation

$$\Delta\mu(c) = -\frac{1}{N}\left(\frac{\partial F_C}{\partial c}\right)_{V,T} \tag{3.19}$$

restated here for convenience. The interface free energy $\Delta F = A\gamma$ was obtained as a function of concentration after subtraction of the tangent.[2]

[1] For a discussion on the proper choice of parameter values see [18]

[2] The tangent construction is described in appendix B.1

5.2 Results

5.2.1 SGC vs. VC-SGC

The difference between SGC and VC-SGC can be seen in Figure 5.1. Note for the SGC ensemble simulation how the standard deviation increases near the binodals and how $\partial F/\partial c$ makes a discontinuous jump through the miscibility gap. The point of discontinuity is somewhat different depending on if the sampling is performed in increasing concentration (forward) or decreasing (backward). This discontinuity stems from the fact that $\partial F/\partial c$ is not one-to-one in the miscibility gap and there are three intersections corresponding to three different concentrations for each value of $\partial F/\partial c$. This failing of the SGC ensemble to produce $\partial F/\partial c$ as a continuous function of the concentration makes it impossible to integrate to obtain the free energy. The VC-SGC data however, which give the same result outside the miscibility gap and with smaller standard deviation, are much more well behaved inside the miscibility gap and are well suited for numerical integration.

5.2.2 Miscibility gap

Figure 5.2 shows the miscibility gap calculated from the free energy as obtained through VC-SGC ensemble simulations. The binodals, where $\frac{\partial \Delta G}{\partial c} = 0$, are indicated with a solid line and the spinodals, where $\frac{\partial^2 \Delta G}{\partial c^2} = 0$ are indicated with a dashed line. The miscibility gap produced via free energy calculations in the VC-SGC ensemble and the phase diagram produced via order parameters are identical. However, it is striking that the phase boundary for the miscibility gap obtained through order parameters does not coincide with the binodals but with the spinodals. The actual configurations however, show that the solubility limit is the binodal.

Complicating things further is the size dependence of the spinodals shown in Figure 5.3. The binodals are size independent since the solubility limit for chromium in iron only depends on the Boltzmann factor where no size dependence enters the calculations. The perceived increase of the miscibility gap for small systems is likely due to the one over square root of size behaviour of the fluctuations and to the large error in concentration if one atom changes species at small sizes. For the spinodals however, the size dependence is obvious and for increasing system size there is no difference between spinodals and binodal.

5.2.3 Interface Free Energy

Figure 5.4 shows the interface free energy as a function of the chromium concentration for an interface area of 6x6xL_z at temperature $T = 2$. The flat region from 0.5 to 0.8 atomic fraction which is particularly pronounced for the 6x6x12 system corresponds to a flat interface. As described in section 3.3.4 and shown graphically in Figure 3.1, the area of a flat interface does not increase with increasing concentration. From Figure 5.4 it is also apparent that

the interface free energy per unit volume decreases as the volume of the size of the system increases.

Figure 5.5 shows a plot of the interface free energy versus the inverse of the length of the system measured in number of unit cells for a flat interface at constant temperature. The expected linear dependence of $\Delta F/N$ as a function of $1/L_z$ from equation (3.26) is confirmed and the value of γ is the slope of the line. Since clusters are dissolved by thermal fluctuations at higher temperatures the interface free energy is expected to approach zero when the temperature increases. This is also confirmed by Figure 5.6 which shows how the interface free energy depends on the temperature. However, the relation between interface free energy and temperature is not trivial. The change of character at temperature $T = 1.5$ can possibly be attributed to the formation of the ordered Heusler phase, but it can also be due to the interfaces forming in different directions, e.g. the [110]- or [111]-directions.

5.2.4 Interface fluctuations

Due to thermal fluctuations the interface is flat only at temperature $T = 0$ while at higher temperatures the interface exhibits roughness. Figure 5.7 shows the chromium concentrations as a function of position along the z-axis along with a fitted error function

$$\operatorname{erf}\left(\frac{x-\mu}{\sigma}\right) = \int_0^{\frac{x-\mu}{\sigma}} e^{-t^2}\,\mathrm{d}t \tag{5.1}$$

The values of σ, which is a measure of the extension of the fluctuations of the interface is seen to increase with temperature. At temperature $T = 4$ there are no precipitates and σ goes to infinity. As temperature goes to zero σ is expected to go to zero but this is numerically difficult to achieve due to the low acceptance probability.

Figure 5.7 also shows the saturation limit of chromium in an iron matrix to the left and the respective saturation limit of iron in a chromium matrix to the right. From the respective saturation limits the miscibility gap can be obtained and is shown by red squares in Figure 5.2.

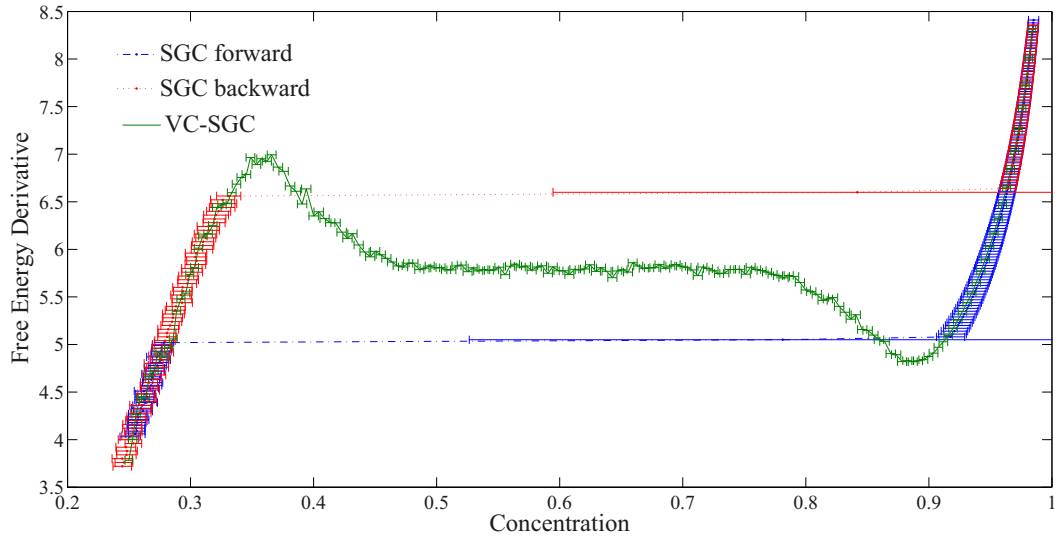

Figure 5.1: *Data obtained through simulations in a SGC ensemble with increasing (blue long dashed) and decreasing (red short dashed) $\Delta\mu$ and in a VC-SGC ensemble with $\kappa = 0.1$ (green solid) at temperature 2 in a system of 6x6x12 unit cells. Note for the SGC ensemble simulations how the standard deviation increases near the binodals and how the free energy derivative makes a discontinuous jump through the miscibility gap. Note also how well behaved the VC-SGC ensemble data are inside the miscibility gap.*

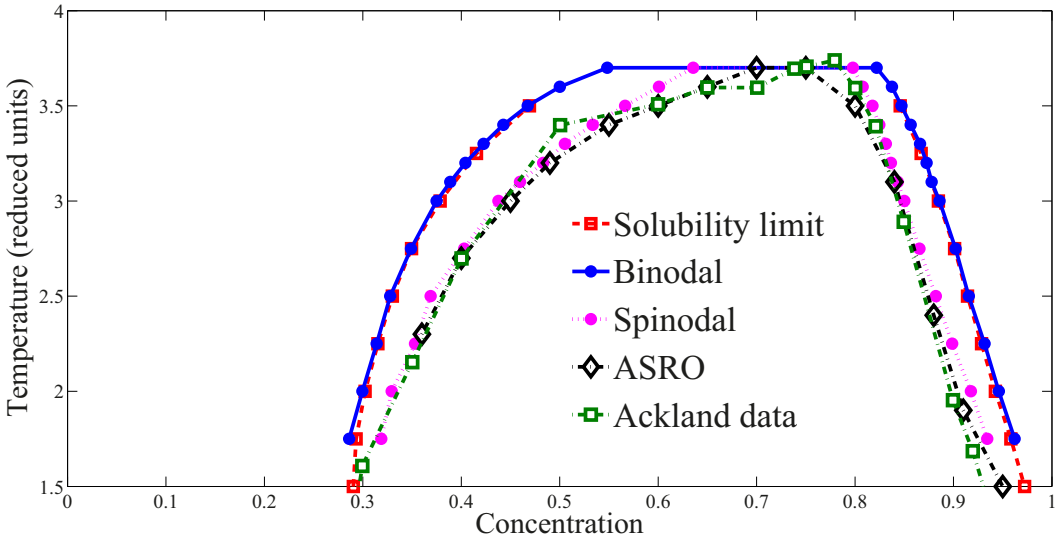

Figure 5.2: *Miscibility gap obtained through calculations of the free energy in a 20^3 bcc supercell. The points connected with a solid line indicates the binodals and the dashed line the spinodals. The line itself has no further significanse than to connect the dots. Note that the spinodals coincide with the values obtained through order parameters indicated with black diamonds and that the binodals coincide with the solubility limit obtained directly from the configurations.*

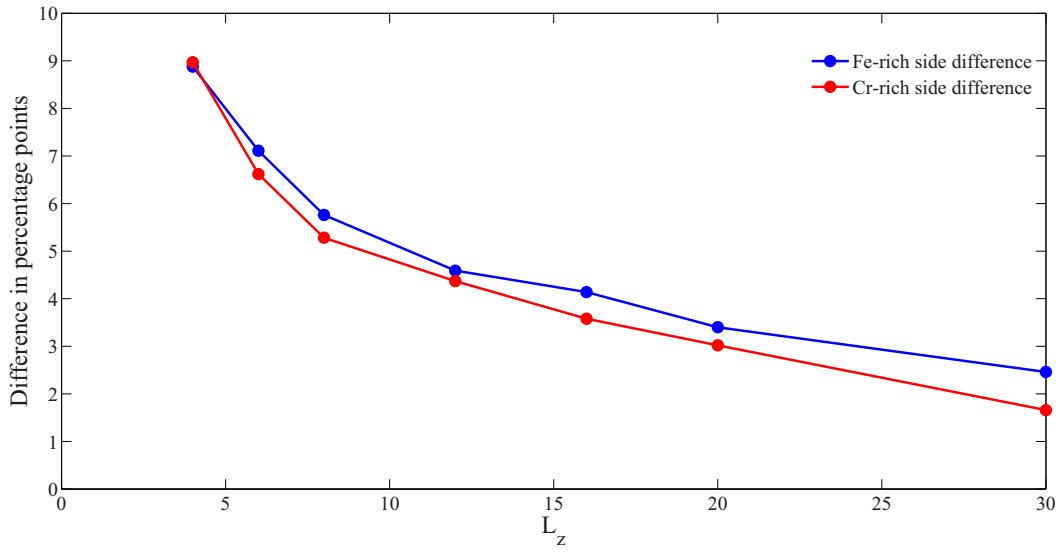

Figure 5.3: *Size dependence of binodals and spinodals in a cubic system generated by a VC-SGC simulation using* $\kappa = 100/N$. *The binodals are found at the same concentrations regardless of the system size while the spinodals are closer together if the size is small and approaches the binodals when the size is increased.*

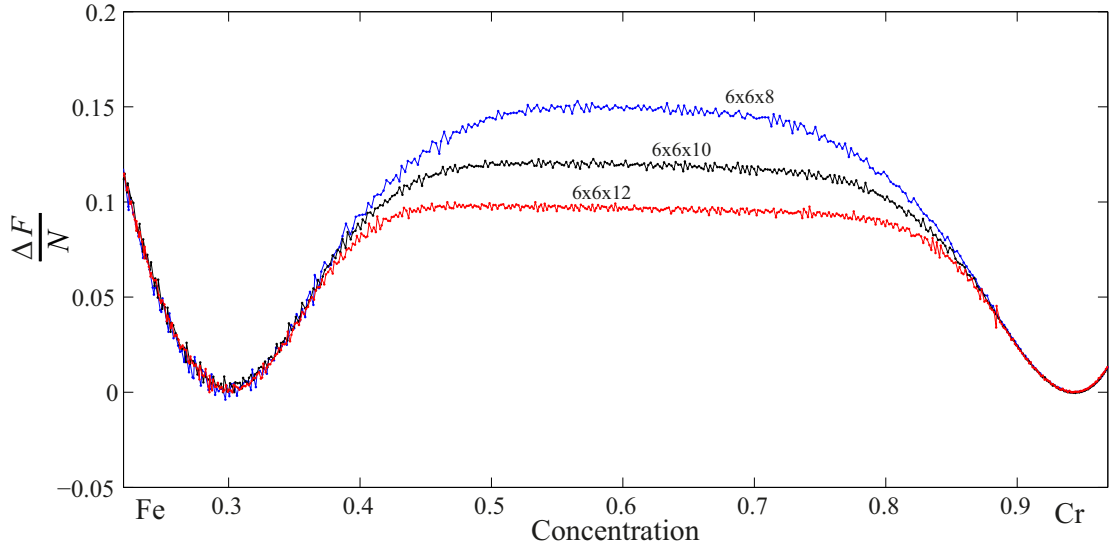

Figure 5.4: *Free energy per unit volume as a function of the chromium concentration at temperature* $T = 2$ *averaged over 100 000 MC steps with* $\kappa = 0.1$. *Note the distinctively flat region between concentrations 0.5 and 0.8 where* $\Delta F/N$ *equals a constant since the interface area remains constant.*

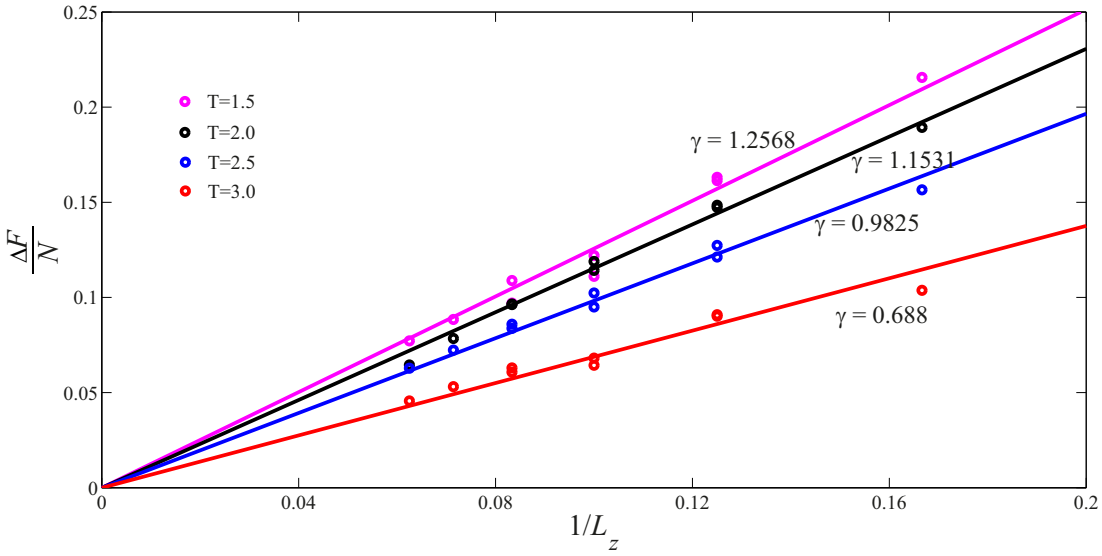

Figure 5.5: *Free energy per unit volume versus the inverse of the extension in the z-direction of the system at temperatures* $T = 1.5, 2, 2.5$ *and* 3*. The figure shows the clear linear dependence of* γ *predicted in equation* (3.26) *and a decrease with increasing temperature.*

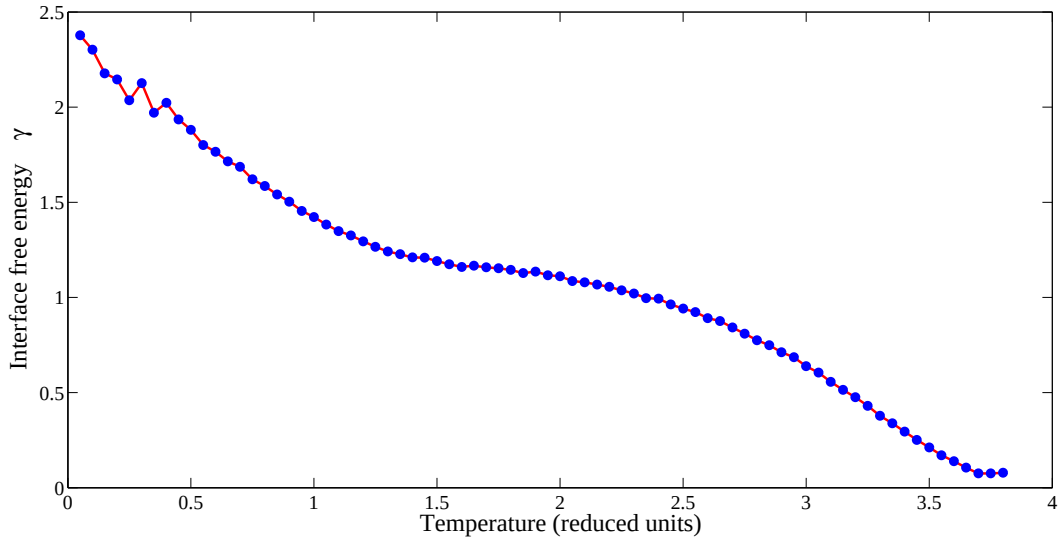

Figure 5.6: *Interface free energy* γ *in the [100]-direction as a function of temperature. Averaged over 5000 MC steps from a 4x4x8 bcc supercell using an additional trial move consisting of both a spin flip and a change of species. The starting configurations were generated through a gradual decrease in Temperature of* $\mathrm{d}T = 0.05$ *from the previous simulation.*

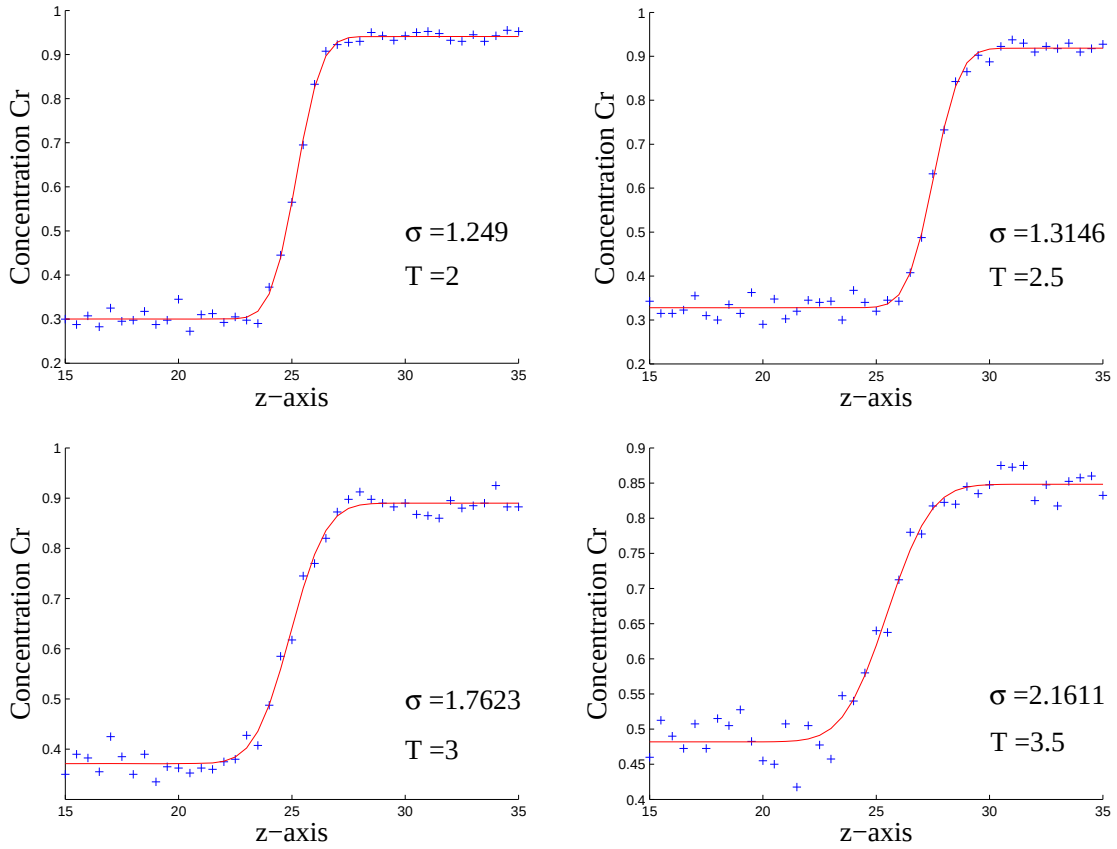

Figure 5.7: *Interface fluctuation for different temperatures. The blue marks show the chromium concentration as a function of L_z and the red curves show fitted error functions for specific configurations.*

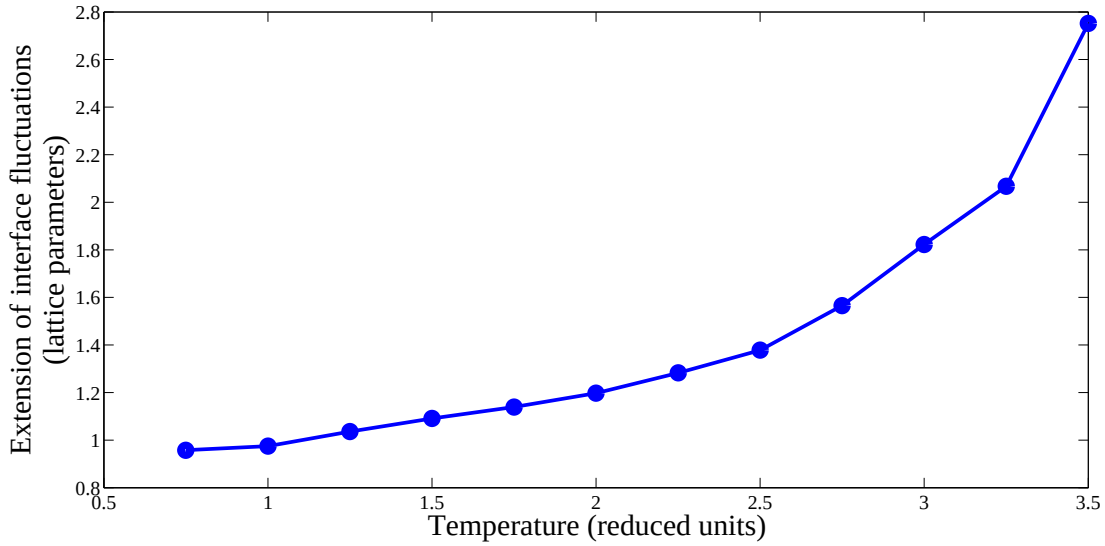

Figure 5.8: *The extension of the interface fluctuations σ measured in number of unit cells as a function of temperature averaged over 20 configurations.*

6 Discussion

The phase diagram obtained by order parameters (Figure 4.9a) exhibits the main characteristics of a Fe-Cr phase diagram in Figure B.3; (i) a Curie temperature and saturation magnetisation which decrease with increasing chromium content, (ii) a miscibility gap skewed towards the right, allowing for solution of chromium in iron at low temperature but not vice versa, and (iii) a ratio between the Curie and the Néel temperatures of 2.9 which is surprisingly close to the measured ratio 3.4. The last property is probably accidental but the other two show that Ising type magnetic effects alone can explain the immiscibility of ferromagnetic and antiferromagnetic type species in a bcc lattice. This is quite remarkable considering the simplicity of the Ising model, that all interaction parameters ε have been set to unity and that no direct repulsive term between iron and chromium has been added.

However, the miscibility gap is somewhat to small compared with the experimental phase diagram. An improvement can be achieved by adding a repulsive term $S_i S_j$ to the Hamiltonian (3.2) [11], by fitting of parameters or by including up to fifth nearest neighbour interaction [12]. Nevertheless, for more quantitatively accurate results an altogether different Hamiltonian would be advisable which, e.g. takes as input data obtained with Density Functional Theory [7, 8, 9, 10].

There is one feature in the phase diagram of Figure 4.9a which is not found in the experimentally observed phase diagram, namely the ordered state of the α-phase at low temperatures. This phase, which we have chosen to call the Heusler phase after its similarity with the ternary Heusler alloy, has not been observed by Ackland [11] despite using the same modified Ising model of equation (3.2). A comparison of the temperature at which the miscibility gap closes with the experimentally obtained phase diagram shows that $T = 1$ corresponds to about 200 K, a temperature at which thermal equilibrium is impossible to obtain. Thus it can be concluded that the Heusler transition cannot be observed experimentally. However, the Heusler transition is most likely a feature of the modified Ising model since it requires a solubility of chromium in iron of 25%.

The low temperature at which this transition takes place also implies a low acceptance probability. In this work the solution has been a rejection of the initial nonequilibrium configurations in combination with a gradual decrease in temperature. Preliminary findings however, show that an additional trial move consisting of a simultaneous spin flip and a change of species could increase the acceptance probability and produce better data for lower temperatures. Another solution could be a trial move of Swendsen-Wang type where whole clusters change spin simultaneously [20].

The phase diagram calculated from the interface free energy, Figure 5.2, shows very good correspondence with the phase diagram obtained from order parameters. However, the miscibility gap obtained from order parameters does not coincide with the binodals as expected but with the spinodals. In the thermodynamic limit, i.e. when the system size goes to infinity, the difference between binodal and spinodal goes to zero, but it can be seen in Figure 5.3 that the rate at which this happens is much slower than assumed by Ackland [11] and for a 20^3 bcc supercell the difference between spinodals and binodals of about 3 percentage points is

too large to be neglected.

The difference between the binodal and the spinodal depends on the critical radius r^* required for nuclei to form. While the binodal marks the onset of the metastable phase region, where clusters constantly form and dissolve without reaching critical radius, the spinodal marks the point beyond which metastable phases can no longer exist and stable clusters form [5]. The order parameter method used by Ackland cannot detect the metastable phase between the binodal and the spinodal, only clusters beyond the spinodal. However, the interface free energy approach proposed by Sadigh and Erhart [18, 21], i.e. Monte Carlo simulations in a VC-SGC ensemble, accurately produces the spinodal as well as the binodal. This is confirmed respectively by the correspondence of spinodals and order parameters and by the correspondence of binodals and solubility limit obtained directly from the sampled configurations. It must be stressed however, that it is important to keep the system size the same in different simulations in order to achieve this correspondance due to the size dependence of the location of the spinodals.

Another indication of the accuracy of the VC-SGC approach is the agreement of the derivative of the interface free energy obtained through simulations of the VC-SGC ensemble with data produced in the SGC ensemble outside the miscibility gap. However, due to the constrained variance in the VC-SGC the fluctuations are, as predicted, smaller compared to the SGC. The good agreement between the two methods outside the miscibility gap suggests that the VC-SGC is a valid generalisation of the SGC for sampling in regions of negative curvature of the free energy.

The flat region in the figure of the interface free energy at intermediate concentrations for systems of cuboid dimensions suggest that flat interfaces are indeed formed and cross correlations with actual configurations support this. The extension of the fluctuations of the interfaces seen in Figure 5.7 and 5.8 are indeed Gaussian and on average zero. The interfaces can therefore be considered flat for intermediate concentrations. The lattice has in this work has been orientated with lattice vectors parallel to the sides of the cuboid system. The flat interfaces have therefore formed in the [100]-direction. By orientating the lattice differently other interface directions can in principle be calculated. Choosing the dimensions of the system differently, e.g. two sides equal and one side shorter could provoke cylindrical interfaces to form. The formation of spherical precipitates, which is the form attained by small clusters, could be found as a $\Delta F \propto c^{2/3}$ behaviour of the free energy at the onset of precipitation. Knowledge of the interface free energy for interfaces orientated in different directions can help explain the shapes attained by clusters in real systems.

7 Conclusions

We have performed Monte Carlo simulations in a ferromagnetic lattice based model of Fe-Cr and obtained a phase diagram which exhibits the main characteristics of the experimentally observed phase diagram. The modified Ising model used shows that ferromagnetic interaction can by itself produce a miscibility gap skewed somewhat to the right, allowing for solution of chromium in iron but not vice versa, even in the absence of a direct repulsive term.

The phase diagram obtained from order parameters in the present work is in close agreement with Ackland's [11] results. The miscibility gap obtained from order parameters was confirmed to correspond to the spinodal by calculations of the free energy but the large difference between spinodals and binodals, even at systems of size 30^3, shows that the assumption of Ackland, that the difference is negligible, is wrong. The present work presents a more accurate way of obtaining the miscibility gap through the interface free energy computed from simulations of a Variance Constrained Semi-Grand Canonical ensemble.

An additional phase transition from ordered state to disordered state at low temperatures and intermediate concentrations has also been found. This ordered phase, which has *Strukturbericht* $L2_1$ and resembles the Heusler Alloy, has not been observed in previous works by Ackland despite using the same modified Ising model.

We have also computed the interface free energy in the [100]-direction of a bcc lattice of Fe-Cr and a predicted relation between system size and interface free energy has been confirmed. A decreasing interface free energy with increasing temperature has also been observed.

References

[1] L. Kaufman and H. Bernstein. "Computer calculation of phase diagrams: with special reference to refractory metals". *Academic Press* (1970).

[2] R. New. "Nickel". *Australian Commodities* 17.3 (2010), pp. 575–579.

[3] F. Garner, M. Toloczko, and B. Sencer. "Comparison of swelling and irradiation creep behavior of fcc-austenitic and bcc-ferritic/martensitic alloys at high neutron exposure". *Journal of Nuclear Materials* 276 (2000), 123–142.

[4] R. Fisher, E. Dulis, and K. CarrolL. "Identification of the Precipitate Accompanying 885-Degrees-F Embrittlement in Chromium Steels". English. *Transactions of the american institute of mining and metallurgical Engineers* 197.5 (1953), 690–695.

[5] J. Cahn. "1967 Institute of Metals Lecture Spinodal Decomposition". *Transactions of the Metallurgical Society of AIME* 242.2 (1968), 166–179.

[6] R. Williams and H. Paxton. "Some Observations on 885-degree-F Embrittlement". English. *Transactions of the American Institute of Minimg and Metallurgical Engineers* 212 (1958), 422–423.

[7] M. Y. Lavrentiev et al. "Monte Carlo study of thermodynamic properties and clustering in the bcc Fe-Cr system". *Physical Review B* 75.1 (2007).

[8] P. Olsson et al. "Ab initio formation energies of Fe-Cr alloys". *Journal of Nuclear Materials* 321.1 (2003), 84–90.

[9] P. Olsson, I. Abrikosov, and J. Wallenius. "Electronic origin of the anomalous stability of Fe-rich bcc Fe-Cr alloys". *Physical Review B* 73.10 (2006).

[10] P. A. Korzhavyi et al. "Electronic structure and effective chemical and magnetic exchange interactions in bcc Fe-Cr alloys". *Physical Review B* 79.5 (2009).

[11] G. J. Ackland. "Magnetically induced immiscibility in the ising model of FeCr stainless steel". *Physical Review Letters* 97.1 (2006).

[12] G. J. Ackland. "Ordered sigma-type phase in the Ising model of Fe-Cr stainless steel". *Physical Review B* 79.9 (2009).

[13] N. Metropolis et al. "Equation of State Calculations by Fast Computing Machines". *Journal of Chemical Physics* 21.6 (1953), 1087–1092.

[14] D. Porter, K. Easterling, and M. Sherif. "Phase transformations in metals and alloys". *CRC Press* (2009).

[15] C. Kittel. "Introduction to solid state physics". *Wiley* (2005).

[16] N. Ashcroft and N. Mermin. "Solid state physics". *Saunders College* (1976).

[17] L. Onsager. *Phys. Rev.* 65 (1944).

[18] B. Sadigh et al. "Scalable parallel Monte Carlo algorithm for atomistic simulations of precipitation in alloys". *Phys. Rev. B* 85.18 (2012).

[19] J. Cowley. "An Approximate Theory of Order on Alloys". *Physical Review* 77.5 (1950), 669–675.

[20] R. Swendsen and J. Wang. "Nonuniversal Critical-Dynamics in Monte-Carlo Simulations". *Physical Review Letters* 58.2 (1987), 86–88.

[21] B. Sadigh and P. Erhart. "Interfacial free energy calculatios via direct thermodynamic integration across phase boundarys". *unpublished material* (2012).

[22] D. Schroeder. "An introduction to thermal physics". *Addison Wesley* (2000).

[23] F. Mandl. "Statistical physics". *Wiley* (1988).

[24] J. Thijssen. "Computational Physics". *Cambridge University Press* (2007).
[25] D. Frenkel and B. Smit. "Understanding Molecular Simulation, Second Edition: From Algorithms to Applications (Computational Science)". *Academic Press* (2001).
[26] J. Rice. "Mathematical statistics and data analysis". *Thomson Brooks* (2007).
[27] T. Massalski et al. "Binary alloy phase diagrams". *American Society for Metals* v. 2 (1986).

A Thermodynamic ensembles

Systems in thermal equilibrium can be characterised by their macroscopic thermodynamic variables, e.g. volume (V), pressure (P) and temperature (T). However, in statistical physics but these quantities are nothing but the time averages of some microscopic configuration in phase space. Statistical physics is the theory of systems with large degrees of freedom and the relation between atomistic degrees of freedom and measurable quantities, the thermodynamic variables.

$$\bar{A} = \lim_{T\to\infty} \frac{1}{T} \int_0^T A(t)\,\mathrm{d}t \tag{A.1}$$

Two very useful theorems from mathematical statistics, the Central Limit Theorem and the Law of Large Numbers, state that when the number of sampled points N go to infinity, or in reality become very large, the distribution of A is Gaussian with the mean value equal to the expected value and a standard deviation $\sigma \propto 1/\sqrt{N}$ [26]. Thus, if N is very large the statistical variable A goes to the thermodynamical quantity $\bar{A}$. This is called the thermodynamical limit. In this context it is also important to realise that not only need the number of samples be very large but for a discrete set, e.g. a lattice model such as the Ising Model, the number of lattice points need to be large in order to reach the thermodynamical limit.

Assuming a system in thermal equilibrium, the physical quantities describing the system macroscopically or controlling the system externally are called *system parameters*. Every set of system parameters correspond to a set of allowed microscopic states. Different experimental circumstances correspond to different system parameters being fixed. These correspond to different *ensembles*. The fundamental postulate of statistical physics is that all microscopic states corresponding to a certain value of the system parameters are equally probable and that every configuration is equally likely to be visited in the course of time (the ergodic hypothesis). This leads to the conclusion that the time average $\bar{A}$ (A.1) is identical to the expectation value

$$\langle A \rangle = \sum_i A_i \mathcal{P}(A_i) \tag{A.2}$$

It should be stressed that this is not true in general and there are examples of systems that do not follow this rule, e.g. glasses and meta stable phases.

A.1 Microcanonical Ensemble

The most fundamental ensemble is the *microcanonical ensemble* or the *NVE-ensemble*, which is described by the number of particles N, the volume V and the energy E. The probability $\mathcal{P}$ of a state is the inverse to the number of states Ω with the prescribed energy.

$$\mathcal{P}(X) = \frac{1}{\Omega(N,V,E)} \tag{A.3}$$

Keeping in mind that the indistinguishability of the particles in the semi-classical model (the interchange of two particles do not correspond to different states) the number of states must also be divided by $N!$. The inclusion of $N!$ also ensures that the entropy defined below is an extensive variable, i.e. scales linearly with system size. (For mixtures, the factor $N!$ is replaced by the product $N_1!N_2!...,$ where the subscripts label different species.) The number of states with the prescribed energy is thus

$$\Omega(N,V,E) = \frac{1}{N!} \sum_X \delta[\mathcal{H}(X) - E] \tag{A.4}$$

where $\mathcal{H}(X)$ is the Hamiltonian which gives the energy at the point X in phase space. We thus have

$$\langle A \rangle = \sum_i A_i \mathcal{P}(A) = \frac{\sum_X A_X \delta[\mathcal{H}(X) - E]}{\sum_X \delta[\mathcal{H}(X) - E]} \tag{A.5}$$

A very important relation is

$$S = k_B \ln \Omega \tag{A.6}$$

which relates the macroscopic entropy to the microscopic multiplicity. The importance of this relation is readily seen as the temperature T, the chemical potential μ and the pressure P are given as derivatives of the entropy with respect to different system parameters

$$\frac{1}{T} = \left(\frac{\partial S}{\partial E}\right)_{N,V} \qquad \frac{\mu}{T} = \left(\frac{\partial S}{\partial N}\right)_{E,V} \qquad \frac{P}{T} = \left(\frac{\partial S}{\partial V}\right)_{E,N} \tag{A.7}$$

as can be readily seen from the first law of thermodynamics, sometimes also called the thermodynamic identity

$$đE = TdS - pdV + \mu dN \tag{A.8}$$

A.2 Canonical Ensemble

In practise it in not the energy that is kept constant but the temperature. This ensemble is called the *canonical ensemble* or the *NVT ensemble* after the system parameters of the ensemble. It can be shown that the probability of a state being occupied under those circumstances is proportional to $\exp\{-\mathcal{H}(X)/k_B T\}$, called the Boltzmann factor. More specifically (with $\beta = 1/(k_B T)$)

$$\mathcal{P}(X) = \frac{1}{N!\, Z} e^{-\beta \mathcal{H}(X)} \tag{A.9}$$

where the partition function

$$Z(N, V, T) = \frac{1}{N!} \sum_X e^{-\beta \mathcal{H}(X)} \tag{A.10}$$

ensures correct normalisation. If the summation is taken only over different energies the partition function takes the following form.

$$Z(N, V, T) = \sum_E e^{-\beta E} \Omega(N, V, E) \tag{A.11}$$

or the more familiar form

$$Z(N, V, T) = \sum_s e^{-\beta E(s)} \tag{A.12}$$

Note that $\mathcal{H}(x)$ counts all the permutations of the state and has to bring along a factor $N!$ whereas $E(s)$ is defined to only count indistinguishable states ones and E (without reference so s) is the energy of the configuration and does not count multiplicities at all. Together with equation (A.6) equation (A.11) can be written as

$$Z(N, V, T) = \sum_E e^{-\beta(E - TS)} = \sum_E e^{-\beta F_E} \tag{A.13}$$

Hence the free energy which in thermodynamical quantities is given by $F \equiv E - TS$ is related to the partition function through

$$F = -k_B T \ln Z(N, V, T) \tag{A.14}$$

Once again the first law of thermodynamics can be used to obtain the following thermodynamic relations

$$\mu = \left(\frac{\partial F}{\partial N}\right)_{V,T} \qquad P = -\left(\frac{\partial F}{\partial V}\right)_{N,T} \qquad S = -\left(\frac{\partial F}{\partial T}\right)_{V,N} \tag{A.15}$$

A.3 Grand Canonical Ensemble

Letting the number of particles vary one obtains the *grand canonical ensemble*

$$\mathcal{P}(X) = -\frac{1}{N!} e^{\beta\mu N} \frac{1}{\mathcal{Z}} e^{-\beta\mathcal{H}(X)} \tag{A.16}$$

$$\begin{aligned} \mathcal{Z}(\mu, V, T) &= \sum_N e^{-\beta\mu N} \frac{1}{N!} \sum_X e^{-\beta\mathcal{H}(X)} = \sum_N e^{-\beta\mu N} Z(N, V, T) \\ &= \sum_N \sum_E e^{-\beta(E_N + \mu N)} \Omega(N, V, E) \end{aligned} \tag{A.17}$$

or in the more familiar form

$$\mathcal{Z}(\mu, V, T) = \sum_N \sum_s e^{-\beta[E(N,s) + \mu N]} \tag{A.18}$$

In analogy with other thermodynamic ensembles one can define a grand canonical potential

$$\mathcal{F}_G = -k_B T \ln \mathcal{Z}_G = F_C - \mu N \tag{A.19}$$

From the grand canonical potential we can therefore derive the thermodynamic relations

$$N = -\left(\frac{\partial \mathcal{F}_G}{\partial \mu}\right)_{V,T} \qquad P = -\left(\frac{\partial \mathcal{F}_G}{\partial V}\right)_{\mu,T} \qquad S = -\left(\frac{\partial \mathcal{F}_G}{\partial T}\right)_{V,\mu} \tag{A.20}$$

A.4 Semi-Grand Canonical Ensemble

For mixtures where the total number of particles is fixed while the concentration is allowed to vary there is a variant of the grand canonical ensemble called the *semi-grand canonical ensemble* defined through the canonical ensemble as

$$\mathcal{Z}_S = \sum_c Z_C \, e^{-\beta \Delta\mu N c} = \sum_c \sum_E e^{-\beta[F_C + \Delta\mu N c]} \tag{A.21}$$

which yields a version of the well-known thermodynamic relation (A.15)

$$\Delta\mu = -\frac{1}{N} \left(\frac{\partial F_C}{\partial c}\right)_{V,T} \tag{A.22}$$

A.5 The Partition Function

From the discussion above it is obvious that the partitions function plays a fundamental role in thermodynamics and statistical physics. We have already seen several examples of this above in equations (A.7), (A.15) and (A.20). But to illustrate the statistical nature of the ensemble approach consider the mean energy of the system $\langle E \rangle$ (often denoted U in thermodynamics) which can be computed as the statistical average (or expectation value)

$$\langle E \rangle = \sum_s E(s) \mathcal{P}_C(s) = \frac{\sum_s E(s) e^{-\beta E(s)}}{\sum_s e^{-\beta E(s)}} = -\frac{\partial \ln Z_C}{\partial \beta} \tag{A.23}$$

and the heat capacity as

$$\begin{aligned} C_V &= \left(\frac{\partial U}{\partial T}\right)_{N,V} = \frac{1}{k_B T^2}\frac{\partial^2 \ln Z_C}{\partial \beta^2} \\ &= \frac{1}{k_B T^2}\left[\frac{\sum_s E(s)^2 e^{-\beta E(s)}}{\sum_s e^{-\beta E(s)}} - \left(\frac{\sum_s E(s) e^{-\beta E(s)}}{\sum_s e^{-\beta E(s)}}\right)^2\right] \\ &= \frac{1}{k_B T^2}\left(\langle E^2\rangle_{NVT} - \langle E\rangle^2_{NVT}\right) \end{aligned} \tag{A.24}$$

where the last expression in round brackets is called the variance of E. Thus if one could obtain the partition function for a system in one could principle derive all thermodynamic quantities from it. However, closed analytical expressions for the partition function are only available in some special cases and the number of allowed states, usually of the order $10^{10^{23}}$, makes it impossible to compute the energy for all states. There are methods available for estimating the partition function numerically, e.g. the Monte Carlo method. The Monte Carlo method allows for a numerical sampling of the average value of thermodynamical quantities, which in turn can be integrated through clever methods to generate the partition function.

B Phase Diagram

A *phase diagram* is a two dimensional map describing the properties of e.g. an alloy subject to different system parameters being held fixed. Often the system parameter on the abscissa is the concentration and on the ordinate the temperature. The boundaries, where equilibrium between different phases exists, appear as lines and the areas enclosed by those lines represent different states or phases of the substance. Examples of such phases are: gaseous, liquid and solid phase, but will in this context refer to different crystal structures or different magnetic properties.

B.1 Construction of the Phase Diagram

A phase diagram can be constructed from the Gibbs free energy G of the system

$$G = H - TS \tag{B.1}$$

Assuming that subsystem A has a Gibbs free energy of G°_A and subsystem B a Gibbs free energy of G°_B then an unmixed combination of the two systems will have a Gibbs free energy of $G_{unmixed} = (1-x)G^\circ_A + xG^\circ_B$, where x is the concentration of B. However, the free energy of the system will not remain constant during the mixing and the actual free energy at concentration x can be expressed

$$G_{mixed} = G_{unmixed} + \Delta G \tag{B.2}$$

where ΔG is the change in the free energy due to the mixing. But, with 1 for the unmixed system and 2 for the mixed system, since $G_1 = H_1 - TS_1$ and $G_2 = H_2 - TS_2$ denoting $\Delta H = H_2 - H_1$ and $\Delta S = S_2 - S_1$ gives

$$\Delta G = \Delta H - T\Delta S \tag{B.3}$$

For an ideal solution, where the free energy change is only due to the change in entropy, $\Delta H = 0$ and ΔS can be written as

$$\Delta S = -R\left[x \ln x + (1-x)\ln(1-x)\right] \tag{B.4}$$

It is important to note that the derivative of ΔS and thus also for ΔG will be infinite at $x = 0$ and $x = 1$ and that the tiniest impurity will lower the free energy regardless of the enthalpy of the system which cannot have an infinite derivative.

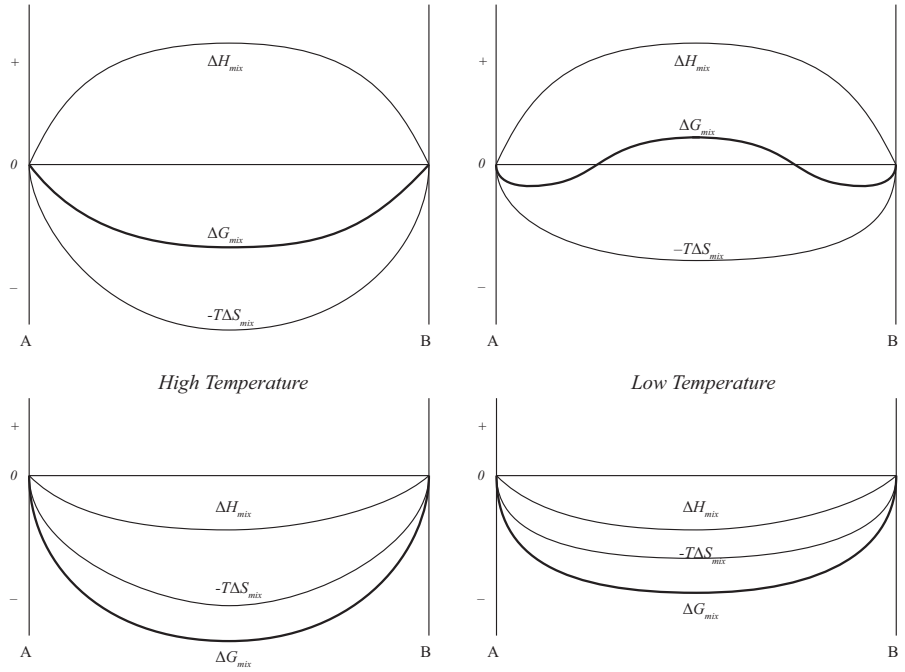

Figure B.1: *Top: The free energy at negative enthalpy $\Delta H < 0$. Bottom: The free energy at positive enthalpy $\Delta H > 0$.*

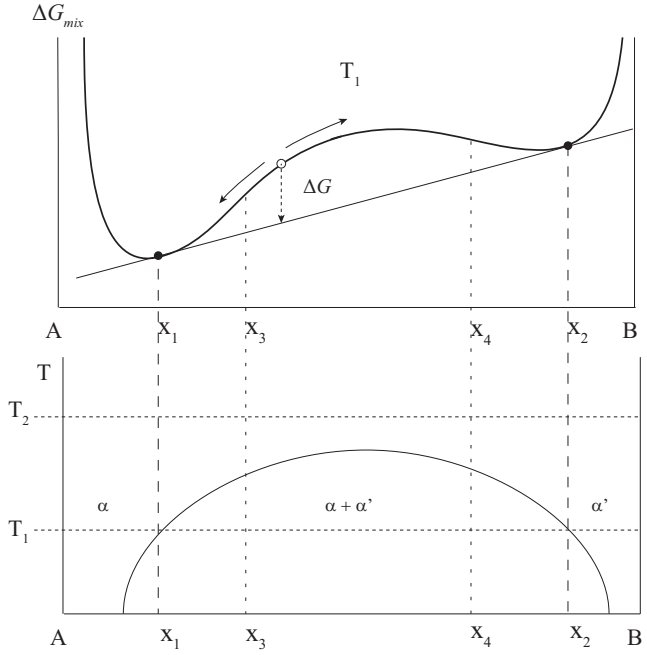

Figure B.2: *Derivation of a phase diagram exhibiting a miscibility gap.*

For $\Delta H < 0$, the lower part of Figure B.1, the free energy is straight forward to obtain as the value where G has a minimum for a given concentration. For $\Delta H > 0$, the upper part of Figure B.1, the case is also straight forward at high temperatures but at low temperatures there is a way to lower the free energy further by phase separation into clusters of concentrations x_1 and x_2. These concentrations, which are the solubility limit of A in B and vice versa, are called *binodals*. Characteristically for a solution with a miscibility gap is that there is a temperature marked T_2 in Figure B.2 where the two species A and B mix before liquid phase occurs. The negative curvature of the free energy between concentrations x_3 and x_4 is an interval which exhibits spontaneous uphill diffusion and spinodal decomposition occurs, a precipitation mechanism which has no barrier for nucleation (see Figure 2.4). The concentrations where $\frac{\partial^2 G}{\partial T^2}$ are called the *spinodals* and are of great importance significance in understanding precipitation in binary alloys.

B.2 The Experimental Phase Diagram of Fe-Cr

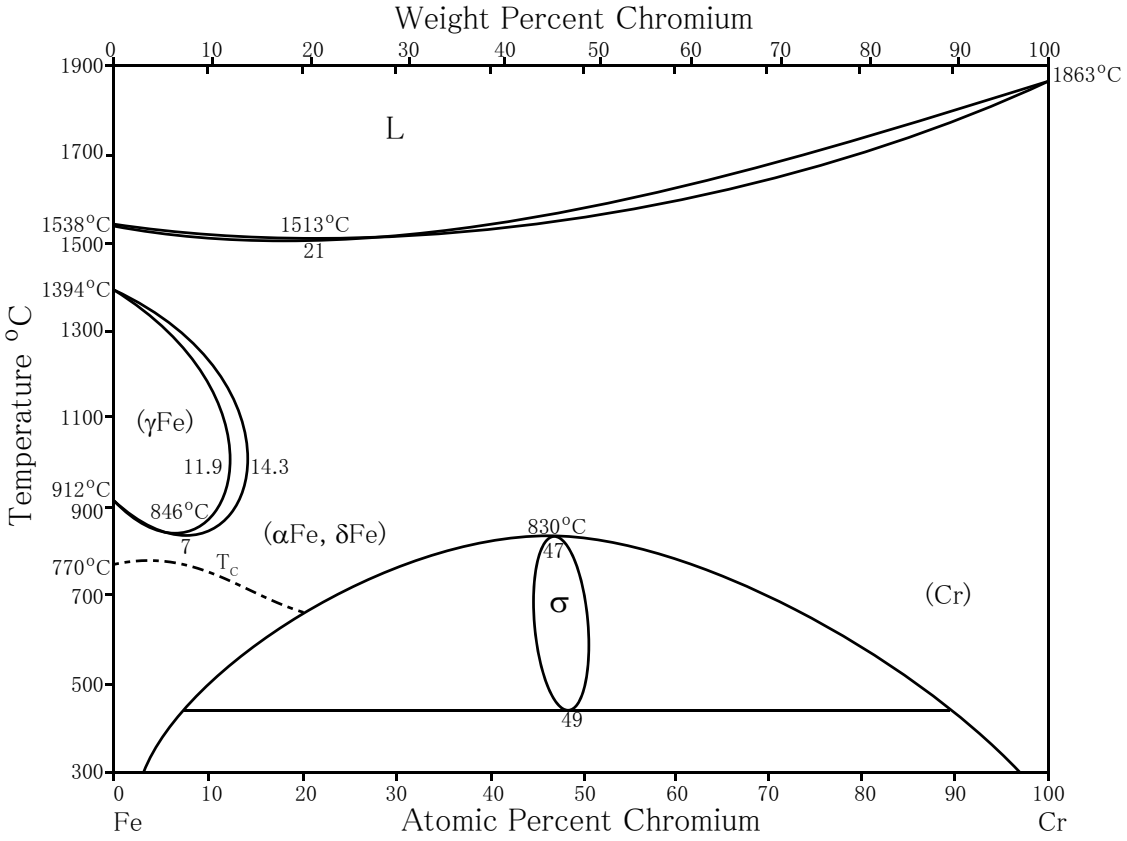

Figure B.3: *The Experimental Phase Diagram of Fe-Cr (redrawn after [27])*

C Phase transitions

Phase transitions happen at critical temperatures T_C and are characterised by changes in internal order of the substance. If L is a measure of this order, essentially two things can happen at T_C. Either L decreases continuously with increasing temperature reaching a value zero at T_C, meaning that the order has disappeared or L can remain virtually constant up to T_C where it drops abruptly to zero. The magnetisation is a typical example of the former and the measure of the order being the magnetisation M. Depending on the behaviour of L near T_C the phase transition is characterised as either first or second order.

A first order phase transition, Figure C.1a, e.g. the melting of a solid, is characterised by a discontinuity in the first derivative of the free energy, e.g.

$$\left(\frac{\partial G}{\partial T}\right)_P = -S \tag{C.1}$$

is discontinuous at the transition from solid to liquid phase. An equivalent formulation is that a first order phase transition is associated with a latent heat. At the phase transition the free energy $G = H - TS$ is constant but the entropy and hence also the enthalpy is greater in the liquid phase causing the heat capacity $C_P = \partial H/\partial T$ to go infinity at the phase transition since heat is supplied at a constant temperature.

A second order phase transition or a continuous phase transition, Figure C.1b, is characterised by a discontinuity of the second derivative of the free energy but a continuous first derivative. This means that the enthalpy H is continuous at the phase transition and consequently

$$\frac{\partial^2 G}{\partial T^2} = -\left(\frac{\partial S}{\partial T}\right)_p = \frac{1}{T}\left(\frac{\partial H}{\partial T}\right)_p = \frac{C_P}{T} \tag{C.2}$$

there is no latent heat, only a high heat capacity associated with the transformation. A second order phase transition is sometimes called a lambda transition due to the shape of the curve of the second derivative.

D Magnetism

Magnetism, being a purely quantum mechanical phenomenon, cannot be fully understood from a classical point of view. However, it is possible to understand many of the properties of magnetism through without going into quantum physics. If a material is subjected to a magnetic field the response of the system can be described as the magnetic susceptibility χ defined as

$$\chi = \frac{M}{B} \tag{D.1}$$

where M is the magnetisation if the material, B is the applied magnetic field. SI-units also require a constant of proportionality of μ_0, the permittivity in free space. Systems with negative susceptibility are called *diamagnetic* and systems with positive susceptibility are called *paramagnetic*. One can show, through a quantum mechanical analysis, that the susceptibility is proportional to T^{-1}. This law, experimentally found by Curie and valid for low magnetic fields or high temperatures, is called the Curie Law and the constant of proportionality, called the Curie constant can be expressed in fundamental constants of nature as

$$C = \frac{NJ(J+1)g^2\mu_B^2}{3k_B} \tag{D.2}$$

where g is the Landé g-factor, μ_B is the Bohr magneton and J is the angular momentum quantum number.

Ferromagnetic materials are systems which display a net magnetisation without externally applied magnetic field. Thus there seems to be an internal magnetic field, an *exchange field* B_E, which does not enter into

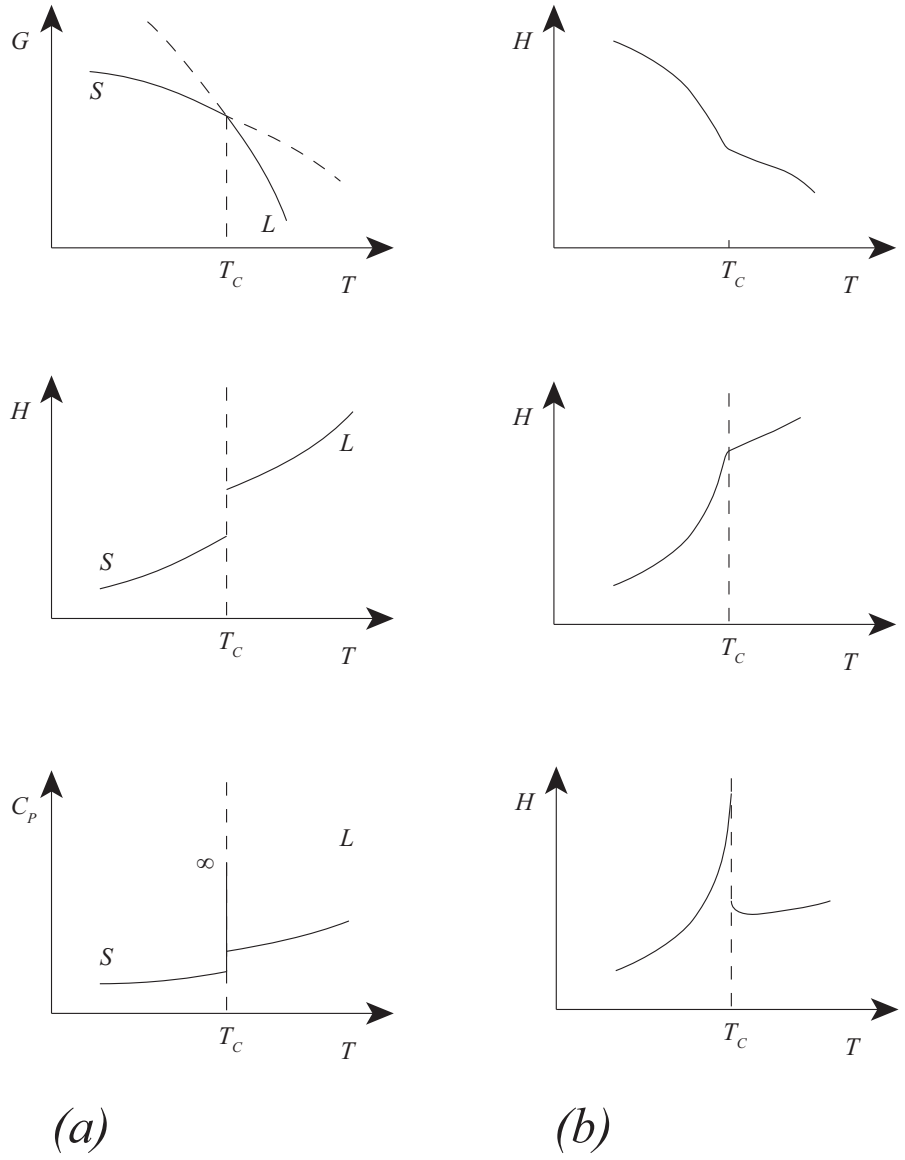

Figure C.1: *Thermodynamic characteristics of (a) first order and (b) second order phase transitions. (Redrawn after [14])*

Maxwell's equations.[1] In a mean field approximation we can macroscopically expect that the exchange field is proportional to the magnetisation, or

$$B_E = \lambda M \tag{D.3}$$

where the constant λ is independent of T. The Curie temperature T_C is defined as the temperature above which the spontaneous magnetisation disappears and the material behaves paramagnetically. Above the Curie temperature we can thus treat the material with Curies law for paramagnetic materials ($\chi_P = C/T$). First we write the magnetisation in terms of the exchange field and the applied magnetic field

$$M = \chi_P(B_A + B_E) \tag{D.4}$$

Once again we drop the constants required in SI-units. Inserting equation (D.3) and the Curie law we can rewrite (D.4) as

$$MT = T\chi(B_A + B_E) = C(B_A + \lambda M) \tag{D.5}$$

The susceptibility will thus become

$$\chi = \frac{M}{B_A} = \frac{C}{T - \lambda C} \tag{D.6}$$

The susceptibility will thus go to infinity at $C\lambda$ which has the dimension of temperature and is the critical temperature or the Curie temperature T_C mentioned above. This is called the Curie-Weiss law.

D.1 The Heisenberg Model

On a microscopic scale magnetism can be regarded as magnetic dipole moments centred on atoms. These are caused by the total angular momentum of the atoms which in general include both a spin and an orbital part, but it is common practise to refer to the these as just spin. On a quantum level in a lattice model the spin coupling between magnetic moments can be described via the Heisenberg model

$$\mathcal{H} = -\frac{1}{2}\sum_{\mathbf{R}\mathbf{R}'} \mathsf{S}(\mathbf{R}) \cdot \mathsf{S}(\mathbf{R}')J(\mathbf{R} - \mathbf{R}') - g\mu_B H \sum_{\mathbf{R}} \mathsf{S}_z(\mathbf{R}) \tag{D.7}$$

The first term is the exchange energy between atoms, where S are quantum mechanical operators, $J(\mathbf{R} - \mathbf{R}')$ is the exchange integral and is related the overlap in the wave functions of the charge distribution. The second term is the energy contribution from en external field, where g is the Landé g-factor, μ_B is the Bohr magneton and H is the externally applied magnetic field.

Although a lot of information about magnetism can be extracted from the Heisenberg model, the complexity of the Hamiltonian limits its uses practically. Many simplifications can be done however, and one of the most important simplification of the Heisenberg model is the Ising model in which $\mathsf{S}(\mathbf{R}$ and $\mathsf{S}\mathbf{R}'$ are assumed parallel or antiparallel.[2] Furthermore, we can assume that $J(\mathbf{R} - \mathbf{R}') = J(\mathbf{R}' - \mathbf{R}) = J_{ij}$ where J_{ij} is equal to zero everywhere except when i and j are neighbours, first neighbours of neighbours of higher order. We also make the assumption that the interaction $J_{ij} = \varepsilon$ is the same for all atoms in the lattice. We then arrive at the Ising model

$$\mathcal{H} = -\varepsilon \sum_{i,j} \sigma_i \sigma_j \tag{D.8}$$

where the sum goes over neighbours i and j.

[1] This is called a Weiss field.

[2] Strictly speaking, since $\mathsf{S}(\mathbf{R}) \cdot \mathsf{S}(\mathbf{R}') = \mathsf{S}_-(\mathbf{R})\mathsf{S}_+(\mathbf{R}') + \mathsf{S}_z(\mathbf{R})\mathsf{S}_z(\mathbf{R}')$ are all quantum mechanical operators dropping the first term $\mathsf{S}_-(\mathbf{R})\mathsf{S}_+(\mathbf{R}')$ from the Heisenberg model gives the Ising model in which $\mathsf{S}_z(\mathbf{R})\mathsf{S}_z(\mathbf{R}')$ commute.

D.2 Magnetic Ordering on a microscopic scale

Just as the macroscopic susceptibility χ can be negative or positive the exchange integral ε can be negative or positive. A positive value of ε will favour parallel spins which will then cause a net magnetisation without externally applied magnetic field, i.e. a *ferromagnetic* material. On the other hand if ε is negative antiparallel spins are favoured. Such a material which i ordered but has a no spontaneous magnetisation is called *antiferromagnetic*.

An antiferromagnetic material will differ from a *paramagnetic* in the sense that while both have zero net magnetisation, a paramagnetic material has random order while an antiferromagnetic material will have its spins aligned antiparallel. Figure D.1 shows possible configurations for an antiferromagnetic structure. The antiferromagnetic structure will look different depending on whether only first neighbour interactions or first *and* second neighbour interactions are considered. For first neighbour interactions the configuration can be visualising as two interpenetrating simple cubic lattices, one with only spin up and the other with only spin down (to the left). The first neighbours are then all in the other lattice. The lowest possible energy per atom will then be -8ε. For first and second nearest neighbour interactions the configuration can be viewed as one chessboard layer on top of another, shifted such that spin up is always straight above spin down, with another chessboard layer between (to the right). The lowest possible energy per atom will then be $(-10+4)\varepsilon = -6\varepsilon$.

While the transition from ferromagnetic to paramagnetic state can be measured through the total magnetisation, $M = \sum \sigma_i$, the transition from antiferromagnetic to paramagnetic cannot, since both have a net magnetisation equal to zero. The difference between the two is on a short range scale and must be measured using short range order parameters such as α_M in section 4.1.2 restated here for convenience.

$$\alpha_M^{(k)} = 1 - \frac{\sigma_+^{(k)}}{\sigma_{tot}^{(k)} \frac{1}{2}(1+M)} \tag{4.4}$$

For $M = 0$ the denominator, which is the expected number of neighbours with spin up, will equal $1/2$ times the number of neighbours. In the case of first and second neighbour interaction the denominator will be equal to 4. In a paramagnetic state this is also the average number of atoms we will encounter with spin up resulting in $\alpha_M = 0$. In a antiferromagnetic state however, the denominator will be 7 while the numerator is 4 resulting in $\alpha_M = 3/7$. In other words, the magnetic SRO parameter will change its value at the critical temperature T_C, the boundary between antiferromagnetic and paramagnetic state.

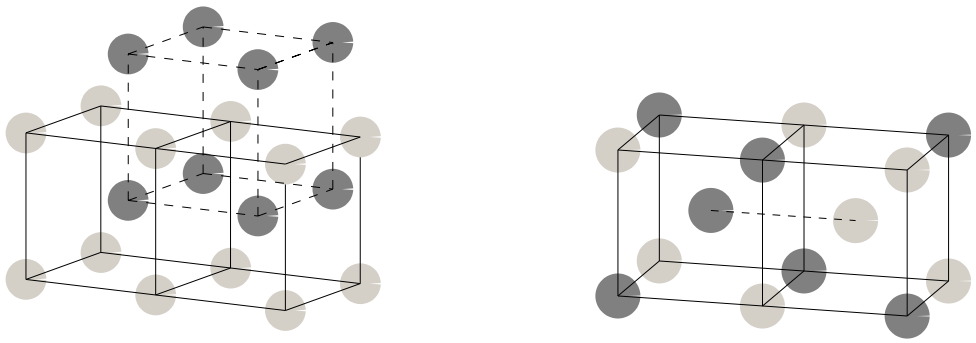

Figure D.1: *Antiferromagnetic structure using first neighbour interaction left and both first and second neighbour interaction right.*